Received: 27 August 2021 | Revised: 5 December 2022 | Accepted: 6 December 2022 | Published on: 16 January 2023

DOI: 10.1002/joc.7983

RESEARCH ARTICLE

International Journal of Climatology RMetS

West Africa's moist convective environment as observed by the Atmospheric InfraRed Sounder (AIRS)

Marian Amoakowaah Osei[1,2] | **Craig R. Ferguson**[3] | **Emmanuel Quansah**[1] | **Michael Padi**[4] | **Leonard K. Amekudzi**[1] | **Sylvester Danuor**[5]

[1]Department of Meteorology and Climate Science, Kwame Nkrumah University of Science and Technology, Kumasi, Ghana

[2]Centre for Ecology and Hydrology, Crowmarsh Gifford, Oxfordshire, UK

[3]Atmospheric Sciences Research Center, University at Albany, State University of New York, Albany, New York, USA

[4]Safety Department, Air Navigation Service, Ghana Civil Aviation Authority, Accra, Ghana

[5]Department of Physics, Kwame Nkrumah University of Science and Technology, Kumasi, Ghana

Correspondence
Marian Amoakowaah Osei, Centre for Ecology and Hydrology, Crowmarsh Gifford, Oxfordshire, OX10 8BB, UK.
Email: marianosans92@gmail.com, marose@ceh.ac.uk

Present address
Marian Amoakowaah Osei, School of Earth and Environment, University of Leeds, Leeds, UK.

Funding information
GCRF African SWIFT project; UK Research and Innovation; Global Challenges Research, Grant/Award Number: NE/P021077/1; Newton International Fellowship, Grant/Award Number: NIF\R1\211183

Abstract

Knowledge of the seasonal positioning of the Intertropical Discontinuity (ITD) is critical to understanding seasonal moist convective processes and associated rainfall over West Africa. This study constitutes a new analysis of the seasonality of moist convection over West Africa, relative to the ITD, based on NASA's Atmospheric Infrared Sounder (AIRS) measurements from 2003 to 2018. Results show that AIRS resolves the seasonal march of the ITD, including its inherent diurnal-scale variations. AIRS captures the north–south daytime skin temperature dipole around the ITD, with greater relative temperatures to the north, especially during March–August. In the vicinity of the nighttime ITD, AIRS profiles indicate increased instability that is characteristic of nocturnal thunderstorm propagation. For seven Ghana weather stations, we show that AIRS positive moisture and equivalent potential temperature anomalies coincide with observed thunderstorm days. On these thunderstorm days, the mean latitude of the AIRS-derived ITD is displaced 3°, 0.2°, and 2° north of its DJF, MAM, and SON climatological positions, respectively, and 1.2° south in JJA. Among four common thunderstorm initiation indices considered, the K-index is determined to be most skillful. The findings of this study contribute to the Global Challenges Research Fund, African Science for Weather Information and Forecasting Techniques project's mission to build local tropical weather forecasting capacity and capabilities in West Africa.

KEYWORDS

AIRS, atmospheric thermodynamics, GCRF African SWIFT, thunderstorms, west African monsoon

1 | INTRODUCTION

West African thunderstorms are the product of a complex interplay of moist convection, a lift mechanism and instability (Parker and Diop-Kane, 2017). In moist convection, the resulting thunderstorm activities over the region can last several days and can lead to the loss of lives and livelihood. Severe thunderstorms, which account for more

than 70% of the region's annual rainfall are often part of larger, more organized mesoscale convective systems (MCSs) that can span an area of 5,000 km^2 (Omotosho *et al.*, 2000; Pante and Knippertz, 2019). The seasonality of severe thunderstorms and MCSs in West Africa are tightly linked to the seasonal latitudinal progression of the Inter-Tropical Discontinuity (ITD), which is a significant feature of the West African Monsoon (WAM; Parker and Diop-Kane (2017)). This ITD is a surface convergence zone between two flows: the moist and relatively cool south-westerly monsoon flow to the south and the dry and warm northeasterly Harmattan flow to the north (Flamant *et al.*, 2009; Bou Karam *et al.*, 2009b; Hastenrath, 2012). The position of the ITD, which can vary from 100–200 km at a diurnal timescale (Pospichal *et al.*, 2010), influences the dynamics of temperature, inland moisture advection and dust emission, which can all affect thunderstorm initiation. On the moist side of the summer daytime ITD, surface temperature inversions are usually observed to be weak, leading to less frequent decoupling from surface friction, less frequent low-level jets, and suppressed moist convection (e.g., Knippertz and Todd (2012)). The ITD propagates northward during the summer (March–August) to approximately 21° N (e.g., Sultan *et al.* (2007)), before retreating southward from September through to the winter (December–February). The height distribution and intensity of ITD-related thunderstorms directly affect upper tropospheric temperature and humidity profiles at larger scales, which are readily observable from satellite instruments. Specifically, the cirrus anvil of these storms imparts a large influence on the regional radiative energy budget (May and Ballinger, 2007).

Given the role that the ITD plays in the organization of moist convection in West Africa, there is a great need to develop a deeper knowledge of the seasonal and inter-annual variability of the ITD. Due to the scarcity of ground observations in West Africa, previous studies of thunderstorm initiation have relied on global atmospheric reanalyses (e.g., Bou Karam *et al.* (2008); Pospichal *et al.* (2010); Roberts *et al.* (2015)). Only a few case studies such as Flamant *et al.* (2009) and Bou Karam *et al.* (2009b) have used surface observations and MODIS-derived total column vertically integrated water vapour content to detect the ITD. NASA's Atmospheric InfraRed Sounder (AIRS), flown on the Aqua satellite since 2002 may offer a more accurate, alternate source of measurement. Namely, AIRS-derived atmospheric stability indices distinguish between stable and unstable regions of the atmosphere in near real-time, which is crucial for detecting severe convective thunderstorms (Menzel *et al.*, 2018). Currently, the full potential of AIRS application over West Africa remains unharnessed and uncharted territory. Out of the three numerical weather prediction models: Integrated Forecasting System (IFS), Weather Research and Forecasting (WRF) and COnsortium for Small-scale Modelling (COSMO), available through the 'synergie' workstation at West African operational weather centres, AIRS radiances are only assimilated into the IFS. AIRS is not assimilated into other models due in-part to the lack of complete uncertainty characterization in West Africa, combined with the lack of investigations into the capability of AIRS in resolving the diurnal-to-seasonal scale anomalies in the moist convective environment of the WAM. Previously, Osei *et al.* (2020), reported that AIRS-derived indices, K-Index (George, 1960), Total Totals index (Miller, 1975) and Humidity Index (Jacovides and Yonetani, 1990), compared well with radiosonde-derived estimates. However, the ability of AIRS to also capture the diurnal and seasonal evolution of WAM, as forced by the movements of the ITD has yet to be explicitly tested.

Therefore, to fulfil in-part the goals of the Global Challenges Research Fund (GCRF) African Science for Weather Information and Forecasting Techniques (SWIFT) project, we assess AIRS's representation of the seasonal WAM progression from 2003 to 2018 through its retrieved profiles of atmospheric temperature and humidity. Evaluation of the performance of AIRS observations of moist convection and stability indices is based on regional expert knowledge from operational weather forecasting and previous studies with other data sources where necessary. To the best of our knowledge, this study is the first of its kind to characterize the region's moist convective environment through the lens of a satellite-based atmospheric sounder. Through demonstrating AIRS capabilities in detecting the motion of seasonal hotspots of moist convection and the ITD, the findings underscore the sensors potential for future integration into operational daily to seasonal forecasting and nowcasting over West Africa. Section 2 gives an overview of the climate of West Africa. Section 3 provides detailed descriptions of data and methods. Section 4 is a summary of main results with discussions. The study's conclusions are presented in Section 5.

2 | STUDY REGION

Figure 1 shows the 16-year (2003–2018) seasonal accumulated mean rainfall (Climate Hazards Group InfraRed Precipitation with Station data [CHIRPS]) and surface air temperature (AIRS) for the study region between longitudes 18.5° W–18.5° E and latitudes 4.5–24.5° N. The annual climate cycle is largely driven by the WAM, which is also forced by the seasonal movement of the ITD (Parker and Diop-Kane, 2017). During DJF (Figure 1a), the accumulated mean rainfall is below 500 mm season^{-1}

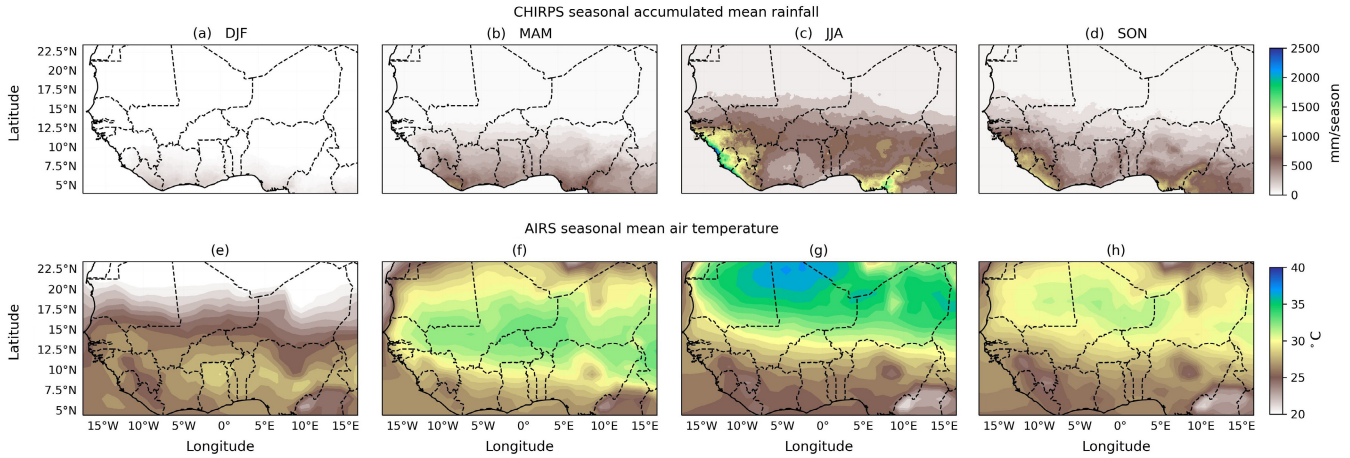

FIGURE 1 CHIRPS seasonal mean rainfall (a–d) and AIRS surface air temperature (e–h) from 2003 to 2018 over West Africa. The mean temperatures represents the average of both descending and ascending overpasses of AIRS for each season

over the entire region. In MAM, rainfall over the Guinea Coast increases to about 1,000 mm season^{-1} (Figure 1b). The seasonal rainfall maximum of around 1,500 mm season^{-1}, occurs in June–August (JJA) along the coast of Guinea and over the Adamawa plateau (Figure 1c). In SON, the accumulated rainfall declines, with maximum over similar locations as in JJA (Figure 1d). For the seasonal mean air temperatures, all of West Africa, have a minimum in DJF (Figure 1e), ranging between 20 and 30°C. During the onset of the monsoon in MAM (Figure 1f), temperatures increase north of 9° N, with a maximum of around 35°C between 12.5° and 18.5° N and 12° W to 6° E. In JJA (Figure 1g), the maximum temperature extends further northward (>15° N), peaking at 40°C. In SON (Figure 1h), the temperature above 12° N declines between 30–35°C. The areas of greatest seasonal rainfall correspond to locations with minimum air temperatures. For instance, in all seasons, the Adamawa plateau (6–8° N, 9–12° E) has the lowest temperature, less than 25°C, but with high rainfall amounts.

3 | DATA AND METHODS

3.1 | Atmospheric InfraRed Sounder

AIRS has been operational since September 2002 aboard the NASA Aqua polar-orbiting satellite. AIRS is cross-track scanning, hyper-spectral resolved, sun-synchronous and has a twice daily global scan with equatorial overpasses at 0130 LT (local time) and 1330 LT for descending and ascending passes, respectively. The sounder gives a holistic, 2,378-channel infrared view of the vertical thermodynamic structure of the atmosphere (Olsen *et al.*, 2017). For the purpose of the present study, AIRS IR-Only Level 3 version 6 algorithm 0.9.0 standard retrieval (AIRS3STD; Susskind *et al.* (2014)) surface air temperature, surface skin temperature, and vertical profiles of mass mixing ratio (MMR) and air temperature were used from January 2003 to December 2018. From the profiles specifically, only data at six standard pressure levels (925, 850, 700, 600, 500, 400 hPa) are analysed here. Since the analysis of this study depended on the correlation between two parameters at different pressure levels, the combined parameter field (TqJoint grids) is used, as recommended by Olsen *et al.* (2017). AIRS3STD includes 1° × 1° resolution global daytime and nighttime overpass maps derived from AIRS Level-2 footprint scale data for which the associated quality flag is either best (0) or good (1) (Olsen *et al.*, 2017). This ensures that only the highest quality retrievals are included, but this biases the AIRS3STD sample towards clear-sky days.

In addition to the thermodynamic fields, AIRS3STD also includes uncertainty estimates (Susskind, 2006). Version 6 cloud-clearing algorithms and uncertainty measures are described in Susskind *et al.* (2014). Figure 2 shows the 2003–2018 mean AIRS Retrieval Algorithm-generated bias estimates for AIRS3STD TqJoint surface air and skin temperatures at 0130 LT (nighttime) and 1330 LT (daytime). The bias of 0130 LT and 1330 LT surface air temperature, and 0130 skin temperature is everywhere less than 3°C. However, during the daytime, uncertainties in skin temperature retrievals increase to 3–6°C in the dry season (DJF) and pre-monsoon (MAM) and 3–5°C in the peak monsoon (JJA) and post-monsoon (SON) seasons. Cloud-cleared estimates of AIRS surface skin temperature showed a regional instrumental bias within ±2°C (Susskind *et al.*, 2019). Similarly, biases in

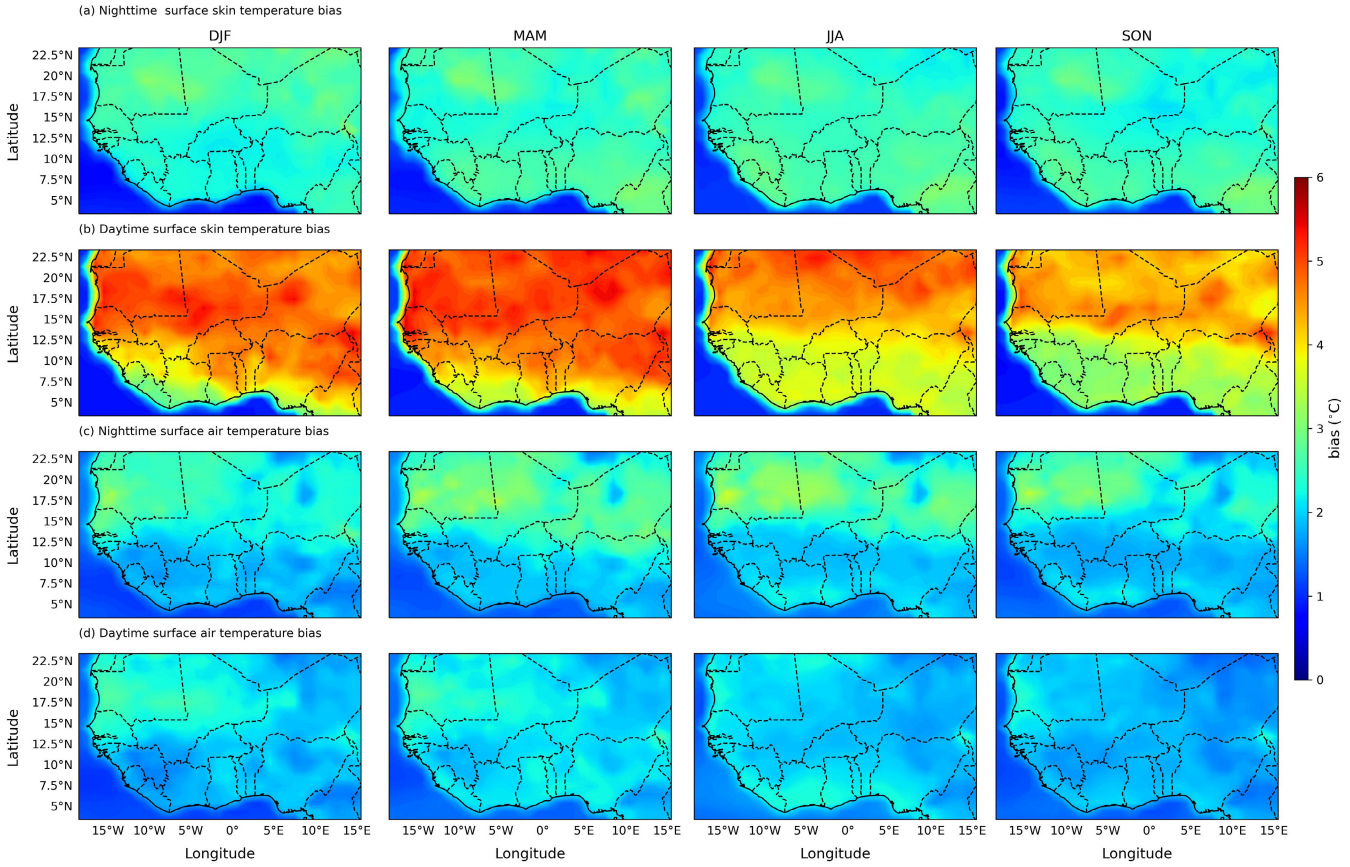

FIGURE 2 The mean AIRS Retrieval Algorithm-generated bias estimates for surface skin and air temperature at AIRS daytime (1330 LT) and nighttime (0130 LT) equatorial overpasses

the vertical profiles of temperature satisfied the AIRS mission accuracy goals of ±1 K, and <20% and <50% for lower and upper tropospheric humidity over West Africa (Osei *et al.*, 2020). Hence, their usefulness as substitutes to radiosonde observations over the region. Recall that AIRS product accuracy is inversely related to cloud fraction. A thorough characterization of AIRS retrieval accuracy under a range of environmental conditions was previously conducted by Ferguson and Wood (2010), which provides further error characterization and attribution.

3.1.1 | Thunderstorm initiation indices

Four thunderstorm initiation indices, commonly used by operational weather forecasters to assess the likelihood of short-term thunderstorm potential were computed using AIRS data. These indices include: K-Index (Equation 1), TT index (Equation 2), HI (Equation 3) and DCI (Equation 4) and are described below.

The K-Index (Equation 1; George (1960)) is a measure of the thickness of low-to-mid-level tropospheric moisture content, where the temperature (T) and dewpoint temperatures (Td) are in degrees Celsius at 850, 700 and 500 hPa pressure levels. K-index thunderstorm likelihood (%) is set at various thresholds which include: ≤20°C (0–20%), 21–25°C (20–40%), 26–30°C (40–60%), 31–35°C (60–80%), 36–40°C (80–90%) and > 40°C (90–100%).

$$K = (T_{850} - T_{500}) + Td_{850} - (T_{700} - Td_{700}) \quad (1)$$

The TT Index (Equation 2; Miller (1975)) is a measure of stability between 850 hPa and 500 hPa levels. It is the sum of vertical totals (T_{850} - T_{500}) and cross totals (Td_{850}–Td_{500}) of temperature and dewpoint temperature. Thunderstorms and severe thunderstorms become more likely when TT index exceed 44 and 50°C respectively.

$$TT = T_{850} + Td_{850} - 2T_{500} \quad (2)$$

The HI in Equation 3 is equal to the mean dewpoint depression at 850-, 700-, and 500 hPa (Jacovides and Yonetani, 1990). Thunderstorm occurrence is likely when HI ≤30°C.

$$HI = (T - Td)_{850} + (T - Td)_{700} + (T - Td)_{500} \quad (3)$$

The Deep Convective Index (DCI; Equation 4) combines the temperature and humidity at 850 hPa and the environmental and parcel temperature (Tp) at 500 hPa (Grieser, 2012). Tp_{500} is computed by raising and cooling the observed temperature at 925 hPa dry adiabatically to saturation, and then cooling it moist adiabatically to 500 hPa. Thunderstorms are possible when the DCI is greater than 30°C.

$$DCI = T_{850} + Td_{850} - T_{500} + Tp_{500} \quad (4)$$

3.2 | Analysis methodology

Analyses were conducted on daytime (i.e., 1330 LT) and nighttime (i.e., 0130 LT) composite means and composite anomalies for each of West Africa's seasons: dry (December to February, DJF), monsoon onset (March to May, MAM), peak monsoon (June to August, JJA) and monsoon cessation (September to October, SON). Specifically, we compared AIRS-derived ITD, equivalent potential temperature (θ_e, K), saturation equivalent potential temperature (θ_{es}, K) and their anomalies, and thunderstorm initiation indices. Seasonal climatologies were also produced for the AIRS surface skin (T_s) and air temperature (T_a) differences, and MMR. The anomalies in equivalent potential temperature (θ_e') and saturation equivalent potential temperature (θ_{es}'), were computed by subtracting at each gridpoint the daily mean value (i.e., 0130 LT and 1330 LT mean) from the seasonal long-term mean (2003–2018). Each vertical profile was averaged over 1° longitude bands, between latitudes 4.5° N and 24.5° N for each season.

Two methods were used to detect the seasonal and annual ITD band: (a) the 10 g·kg^{-1} specific humidity (converted from AIRS MMR) at 925 hPa (q925) and (b) the 14°C dewpoint temperature at 925 hPa (Td925). Currently, it is inconclusive which method works best, but according to Roberts *et al.* (2015), the q925 hPa (10 g·kg^{-1}) metric is relatively drier than the surface Td925 (14°C), and may be a useful indicator of the large-scale latitude to which moisture is advected by the monsoonal flow. The 14°C (Td925) criterion has air to the north (south) of the ITD being characterized by dewpoint temperatures less than (in excess of) 14°C and northerly to easterly (southerly to westerly) winds (see Bou Karam *et al.* (2009a)). On inter-annual scales, the latitudinal positions of the ITD were determined by first averaging the computed q925 and Td925 across longitudes 18.5° W - 18.5° E, which transformed the data from 3-dimensional to 2-dimensional (latitude and q925 (Td925)), and then identifying the latitude for which q925 and Td925 were 10 g·kg^{-1} and 14°C respectively using linear interpolation. Equations 5 and 6 were used to compute the 925 hPa specific humidity (q) in g· kg^{-1} and dewpoint temperature (Td) in °C respectively, where, 'e' is the vapour pressure in hPa (Bolton, 1980).

$$q = \frac{MMR}{1 + MMR} \quad (5)$$

$$Td = \frac{243.5 log(e/6.122)}{17.67 - log(e/6.112)} \quad (6)$$

Thunderstorm-conditional sample statistics, based on weather observer reports from 2003 to 2009 and 2015 to 2018 at seven synoptic stations in Ghana (see Table 1 for station descriptions), namely; Accra, Saltpond, Ho, Kumasi, Wenchi, Bole and Tamale were computed and compared with the corresponding AIRS 1330 LT daytime seasonal mean ITD for the thunderstorm years. After computation, the seasonal mean ITD positions during the thunderstorm years were similar to the AIRS 16-year (2003–2018) seasonal mean ITDs, hence all discussions are made relative to the latter. The 1330 LT equatorial overpass of AIRS was used because convection usually peaks over Ghana and West Africa between 1400–1500 LT (Parker and Diop-Kane, 2017; Aryee *et al.*, 2019). The conditional sample statistics calculated include seasonal composite means and anomalies for MMR, θ_e and the ITD on thunderstorm days. Here also, we computed the meridional arc between the station latitude and ITD location for the seasonal thunderstorm days by calculating the mean of the q925 and Td925 variables, averaging longitudes 4.5° W and 1.5° E and using linear interpolation to detect the mean latitudinal location of the 10 g·kg^{-1} and 14°C contours. After this, the latitude of the ITD is subtracted from the station latitude using a simple differencing equation (station_latitude - ITD_latitude). In addition, we obtained for each thunderstorm initiation index, the mean seasonal threshold of occurrence at all stations and compared with the general thresholds of the K-index, TT-index, HI and DCI. The seasonal thresholds were computed by averaging for each season and station the indices on the thunderstorm days. This led to a single index value for each season and station (7 stations × 4 seasons), which were transformed into scatterplots.

Analysis variables were selected for their respective role in tropical moist convective processes. Skin and air temperature differences influence the potential for convective activities under tropical humid climate (Jin *et al.*, 1997). Apart from the surface skin temperature

TABLE 1 Station coordinates, elevation (metres above mean sea level), combined 2003–2009 and 2015–2018 thunderstorm (TS) day count, and mean offset in degrees along a meridian arc between station latitude and the AIRS q925 (Td925)-derived ITD latitude on observer-confirmed thunderstorm days

Stations	Location	Elevation	TS count	DJF	MAM	JJA	SON
Accra	0.18° W, 5.60° N	61	255	2.5 (1.9)	5.8 (5.0)	9.4 (9.3)	7.7 (6.7)
Saltpond	1.05° W, 5.20° N	1	327	3.0 (2.2)	6.6 (5.8)	9.9 (9.3)	7.5 (6.3)
Ho	0.47° E, 6.61° N	150	565	2.2 (1.4)	4.5 (3.8)	10.1 (9.2)	8.2 (7.2)
Kumasi	1.61° W, 6.66° N	250	721	2.3 (1.4)	4.6 (3.9)	9.9 (9.2)	7.6 (6.7)
Wenchi	2.10° W, 7.74° N	304	590	1.5 (0.6)	3.7 (3.0)	8.9 (8.9)	6.6 (5.5)
Bole	2.48° W, 9.03° N	296	456	0.5 (−1.0)	3.3 (2.4)	8.2 (7.3)	6.9 (5.8)
Tamale	0.84° W, 9.40° N	151	673	0.1 (−0.8)	2.8 (2.1)	8.2 (7.3)	7.0 (5.9)

being a proxy for climate change, its diurnal cycle is essential for the computation of surface energy partitioning into sensible and latent heat fluxes. Specifically, the sensible heat flux is determined as a function of the instantaneous difference between the surface skin and near surface temperatures. In the presence of sufficient moisture and increasing surface air temperature, ascent of moist warm air increases the conservative θ_e, which encapsulate latent heat releases from air parcels. Thus, an indication of positive buoyancy can be inferred and the corresponding regions of elevated θ_e serve as sources for thermodynamically-induced thunderstorms and MCSs (Sikora, 1976; Thorncroft *et al.*, 2003; Giaiotti *et al.*, 2007; Georgiev *et al.*, 2016). Son and Seo (2020) showed that lower tropospheric T_a and θ_e could explain the initiation of deep convection over the Guinea Coast. The development of a strong gradient in the lower atmospheric θ_e corresponds to vertical ascent in the lower troposphere, positive vorticity in the middle troposphere and vertical ascent south of the coast. On the other hand, θ_{es} (also conserved), is useful for indicating moist convective regimes through a region's conditional instability (see Akinsanola and Ogunjobi (2013); Parker *et al.* (2016)). It is dependent on the air temperature at a pressure level, where a constant profile with height is consistent with pseudoadiabatic processes and moist adjustment by convective clouds (Parker *et al.*, 2016). Oduro-Afriyie (1989), using 100 surface stations over West Africa for 1977, and Omotosho (1984), found that monthly θ_e and θ_e' can serve as proxies for determining the onset and cessation of the monsoon rains over the region. But, these studies were performed either at a single station (Omotosho *et al.*, 2000) or short time-period (1-year, Omotosho (1984); Oduro-Afriyie (1989)).

AIRS-derived variables including q925, Td925, θ_e and θ_{es} were computed using MetPy version 1.3 (May *et al.*, 2022) based on Equations 5–8 (Holton, 1973) respectively. In the equations, T_a is the temperature of air (K) at pressure p, p_o and p are the reference/initial and final pressures (hPa) respectively, R_d is the specific gas constant for dry air ($J/[kgK]$), c_p is the specific heat of dry air at constant pressure ($J/[kgK]$), L_v is the latent heat of vaporization ($kJ/[kg]$), w_s is saturation mixing ratio respectively.

$$\theta_e \approx \left(T_a + \frac{L_v}{c_p} MMR\right)\left(\frac{p_o}{p}\right)^{\frac{R_d}{c_p}} \tag{7}$$

$$\theta_{es} \approx \theta \exp\left(\frac{L_v w_s}{c_p T_a}\right) \tag{8}$$

4 | RESULTS AND DISCUSSIONS

This section is split into two distinct analyses which include the spatio-temporal variabilities in the AIRS thermodynamic variables and the station-based analyses from the thunderstorm conditional sampling at selected weather stations in Ghana. The regional analyses are conducted over longitudes 18.5° W–18.5° E and latitudes 4.5° N–24.5° N.

4.1 | Seasonal and annual AIRS-derived ITD over West Africa

The mean seasonal migration of the AIRS-derived ITD is shown in Figure 3. Both AIRS nighttime and daytime ITDs depict the intermediate nodes between the expected times of peak at 0600 LT and 1800 LT respectively, observed at operational West African meteorological centres. Conventionally, the daytime ITD is known to be situated further south of its nighttime position (Parker and Diop-Kane, 2017). For all seasons, the ITD location, as mapped by the 925 hPa 10 g·kg^{-1} specific humidity (blue;

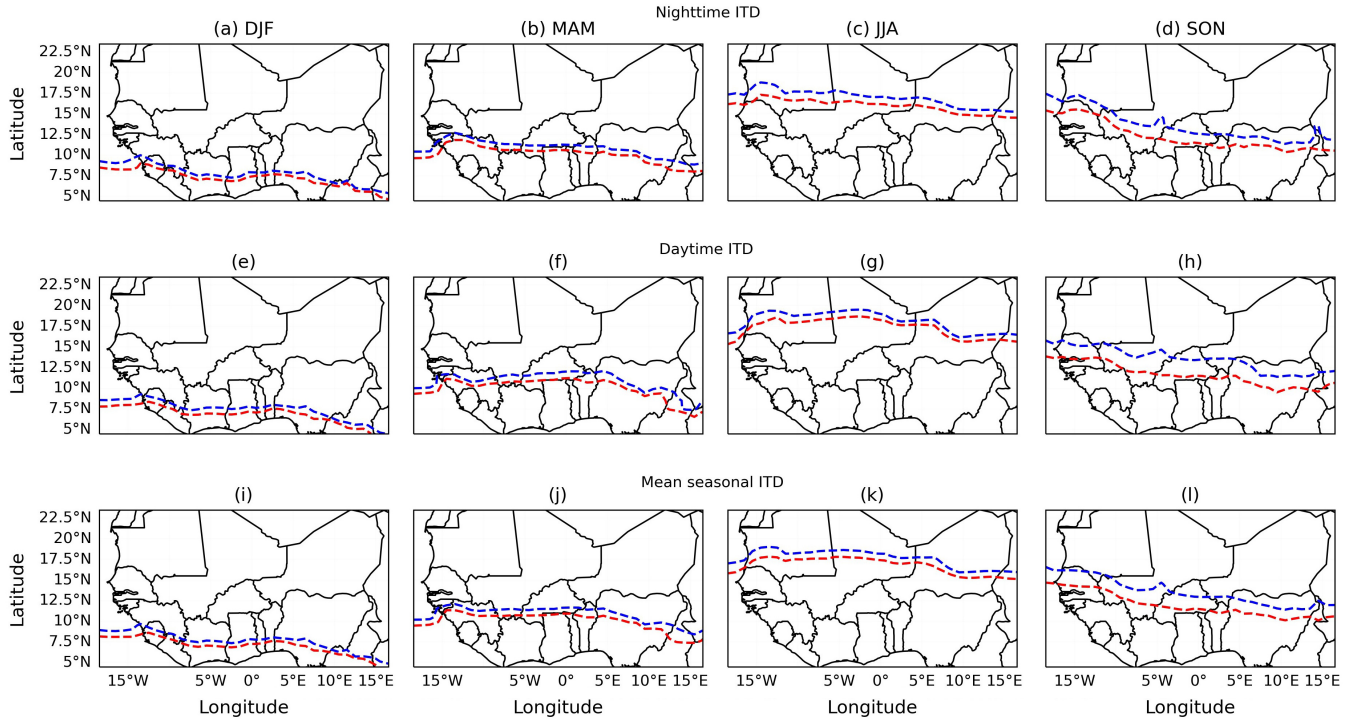

FIGURE 3 Mean seasonal propagation of the AIRS-derived ITD using the 10 $g \cdot kg^{-1}$ specific humidity (blue) and 14°C dewpoint temperature (red) contours at 925 hPa from 2003–2018. The contours are for the nighttime (0130 LT, panels a–d), daytime (1330 LT, panels e–h) and the diurnal mean in panels i–l.

hereafter q925) contour and 14°C dewpoint temperature (red; hereafter Td925) contour, follow the same seasonality. However, the 10 $g \cdot kg^{-1}$ specific humidity contour lie about 1° north of the 14°C dewpoint temperature contour. The spatial disparity in the two indices become more prominent in the daytime SON (Figure 3h), where the latitudinal difference in q925 and Td925 increases to about 2°–3°. Latitudinal variability in the spatial structure of the ITD is less pronounced during JJA (Figures 3c,g), when the ITD is at its Northern-most position. The positions of the nighttime ITD-Td925 between longitudes 6° W and 12° E in MAM is similar to that found by Pospichal *et al.* (2010) in April 2006 at 0200 LT from Meso-NH and ECMWF dewpoint temperature analyses. Comparison of AIRS-derived ITD-q925 in Figures 3j–l with the ITD-q925 derived in the work of Roberts *et al.* (2015) using seven model simulations (CFSR, GFS, NCEP-NCAR, NCEP-DOE, MERRA, ERA-Interim and ERA-Operational) for the year 2010, show an agreement with CFSR, GFS and NCEP-NCAR in MAM with mean position between 9° N and 12° N and all except MERRA, ERA-Interim and ERA-Operational in JJA when the mean position lies between 15° N and 20° N. Meanwhile, Bou Karam *et al.* (2009b) estimated the ITD using large differences in MODIS integrated water vapour content for seventh and eighth July 2010 at 1030 LT. On these days, the MODIS-derived ITD was averagely located around 17° N, which is about 1° south of the AIRS-derived daytime ITD-q925 and similar to ITD-Td925 (see Figure 3g).

The more northern location of the q925 and Td925 ITDs, averaged across longitudes 18.5° W to 18.5° E are also observed in Figure 4. Here, the difference in ITD q925 and Td925 persists with mean values of 2.5° in the night and 1.5° in the daytime (Figure 4a). For ITD-q925, nighttime mean peaked in 2012 as opposed to 2016 for the daytime ITD-q925. The inter-annual averages also show most years observed a higher nighttime ITD-q925 than the daytime, which conforms to general observations from studies on its dynamics (Parker and Diop-Kane, 2017). Meanwhile, daytime ITD-q925 was lowest in 2008 (10.5° N; Figure 4a), with a −0.8° anomaly (Figure 4b) and 1σ below normal (Figure 4c). This reflected in a 0.5σ below normal MMR at 925 hPa (not shown) in 2008, which may be attributed to a weakened moonsoonal flow or decreased MCSs activity in the year. Alternatively, for ITD-Td925, both night and day times locations varied between 9° N and 10.5° N. Nighttime ITD-Td925, shows a steady decline from 2003 to 2018 (Figure 4a). Meanwhile, the daytime ITD-Td925, which lies north of the nighttime ITD was in quasi-steady state. The anomalies in Td925 ITDs were quite low with ranges between ±0.2° from the mean (Figure 4b). Between 2003–2010, the anomalies in AIRS ITD-q925 lie within

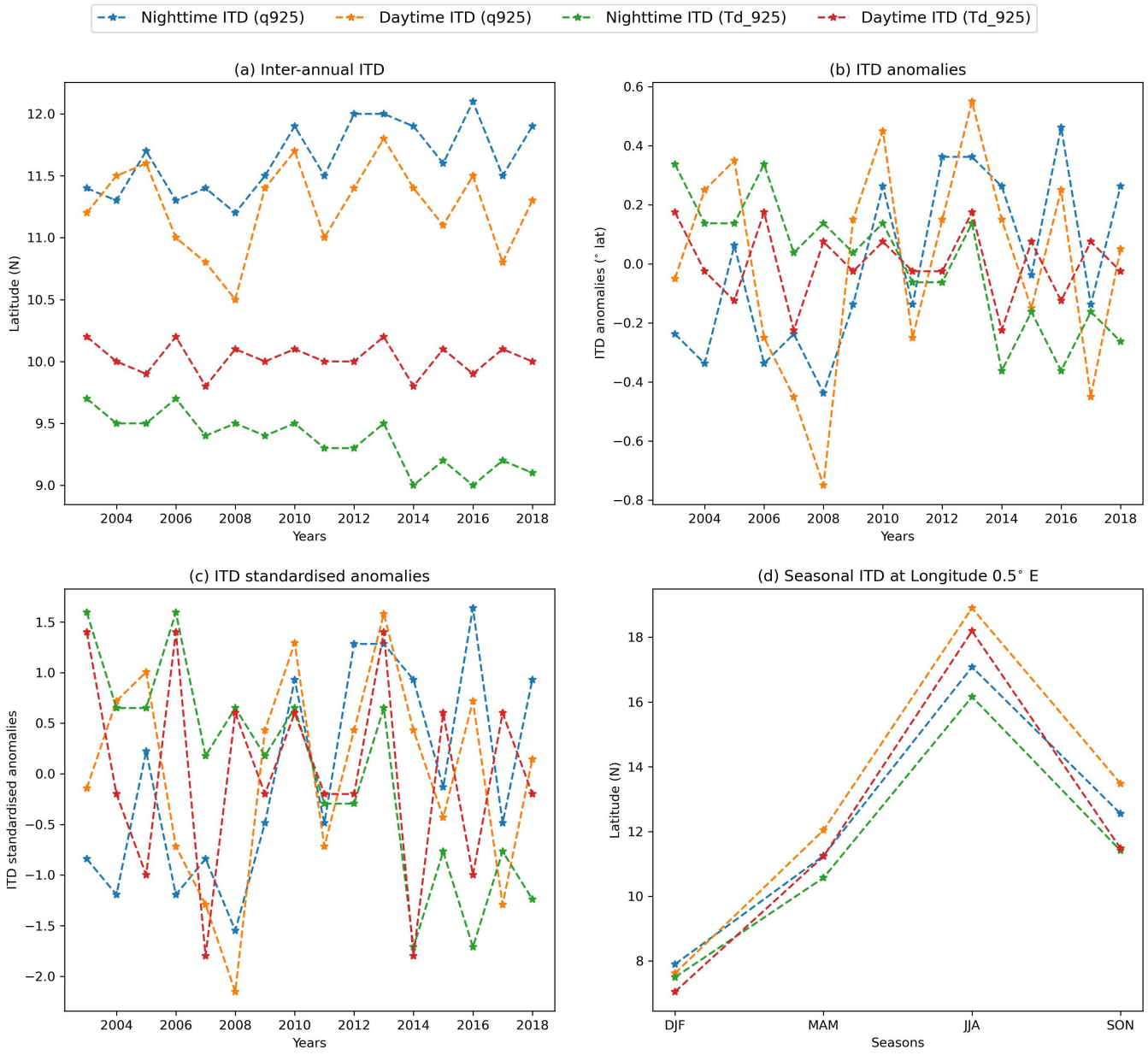

FIGURE 4 AIRS q925- and Td925-derived 2003–2018 ITD (a) annual mean latitude, (b) annual mean latitudinal anomaly, (c) standardized annual mean latitudinal anomaly, and (d) seasonal mean latitudinal location at 0.5° E for nighttime (0130 LT) and daytime (1330 LT) overpasses

±1° band observed by almost all the seven models used by Roberts *et al.* (2015). The extreme inter-annual anomalies (Figures 4b,c) in the diurnal and nocturnal ITD-q925 may be due to a high sensitivity of the metric to water vapour (relatively drier), as compared to ITD-Td925 metric (Roberts *et al.*, 2015). Finally, based on a reference coordinate (longitude 0.5° E; Figure 4d), we quantified the departure of the two ITD methods on the seasonal timescale for both day and night. The daytime AIRS-derived ITDs for q925 and Td925 both show the northernmost limit in JJA to be around 18.2° N and 18° N respectively. The nighttime ITDs on the other hand, lie about 1°–2° south of the daytime ITDs in both methods. However, there is a close agreement in the methods during the dry season (DJF), with nighttime ITDs slightly northward than the daytime (following the generally observations).

4.2 | AIRS mass mixing ratio (MMR)

Figure 5 shows the seasonal mean variation of the mass mixing ratio at pressure levels from 925 hPa to 400 hPa, and also indicates the depth and latitudinal range over which atmospheric moisture is transported seasonally.

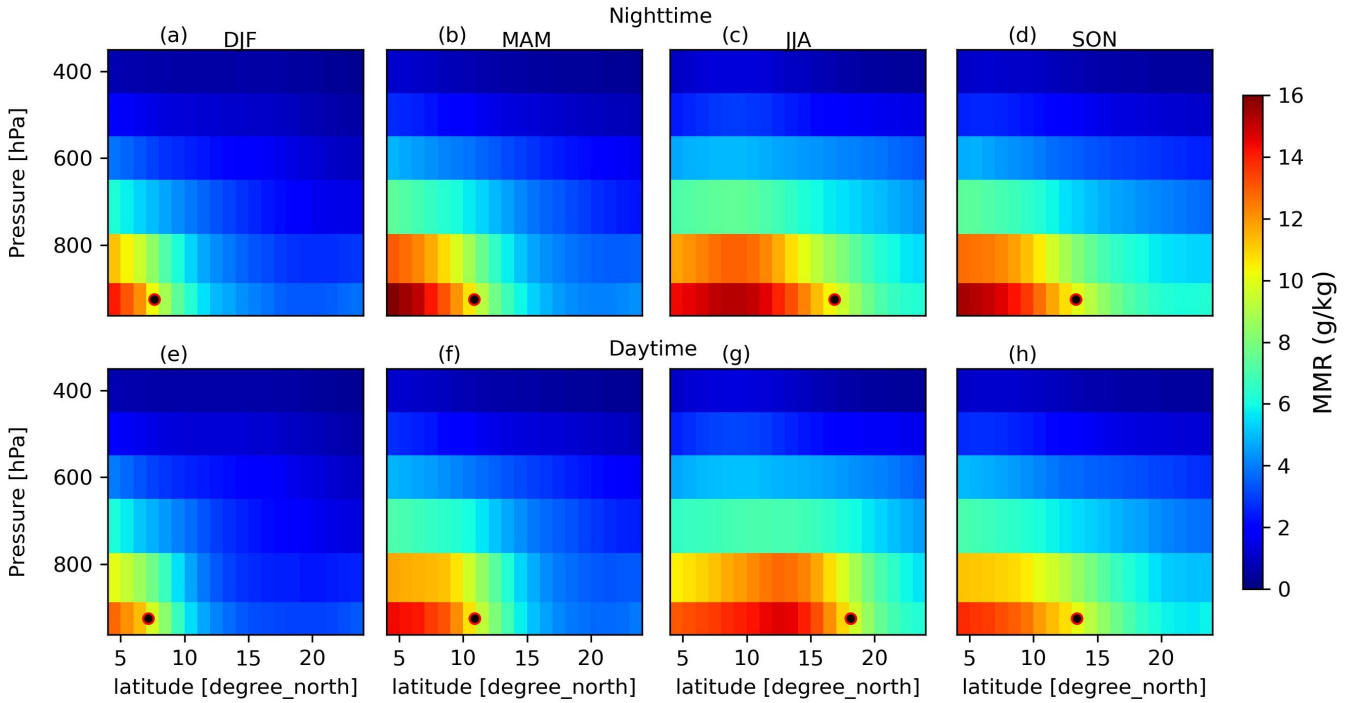

FIGURE 5 Seasonal mean of the mass mixing ratio over West Africa at AIRS nominal overpass for nighttime (0130 LT, a–d) and daytime (1330 LT, e–h) from 2003 to 2018. The seasonal latitudinal mean is calculated across longitudes 18.5° W–18.5° E. The climatic divisions of West Africa across latitudes include: 4–8° N (Guinea Coast), 8–12° N (Savanna) and >12° N (Sahel). The circular dot shows the mean location of the ITD for the season based on 10 $g \cdot kg^{-1}$ from q925

The moisture depth in DJF increases from the surface to about 700 hPa along the coast (Figures 5a,e). The humidity between 850–700 hPa decreases sharply from about 5° N to 10° N (Figures 5a,e). North of 11° N, the troposphere is relatively dry with MMR falling below 5 $g \cdot kg^{-1}$ in both day and night. By the pre-monsoon season (MAM), moisture penetrates slightly northwards (15° N) with a maximum magnitude at 925 hPa of 16 $g \cdot kg^{-1}$ (Figures 5b,f). In JJA, maximum moisture content resides between 7° N and 10° N (16 $g \cdot kg^{-1}$; Figure 5c) during the night and 8°–15° N (14 $g \cdot kg^{-1}$; Figure 5g) during the day. Moderate to relatively dry moisture content also extends over the entire region at the midlevels (i.e., 700–600 hPa) in JJA as compared to DJF and MAM. The usually drier mid-troposphere is a product of the drier winds of the African Easterly Jet (AEJ; Parker and Diop-Kane (2017)). In SON, the highest levels of humidity are found equatorward near the Guinea Coast (Figures 5d,h). Meanwhile, at the middle to upper troposphere, above 600 hPa, low moisture is observed in all seasons. Although north of the ITD is usually relatively dry, from Figure 5, low- to-mid-tropospheric moisture of about 6 $g \cdot kg^{-1}$ accelerates to about 4° north of the ITD for all seasons. In addition, the nighttime maximum MMR is always located about 4° south of the ITD (Figures 5a-d).

The magnitude of moisture depth is higher during the night than at daytime due to the roles of the nocturnal low-level jet (NLLJ) and the northward displacement of the ITD at night. The NLLJ aids horizontal cold air advection, which is crucial in the formation of low-level clouds (Aryee *et al.*, 2021). Cool monsoonal air to the south of the ITD also speeds northward during the night when boundary layer mixing is poor, boosted by these nocturnal low-level jets. Therefore, stations north of the Sahel that endured hot, dry afternoons with light breezes receive cooler, moister winds overnight as these southerlies arrive (Lothon *et al.*, 2008; Parker and Diop-Kane, 2017). As previously stated from Figure 3, the northward migration of the AIRS-derived ITD is not fully established over the region due to time anomaly between the descending overpass time (0130 LT) and the operational time-of-peak of the nocturnal ITD at 0600 LT. Hence, although moisture depth is enhanced during the night from Figures 5a-d, the nocturnal flow is still yet to be fully established for the northward acceleration of the ITD, which peaks at 0600 LT.

4.3 | AIRS surface skin and air temperature

Figure 6 shows the seasonal variability in AIRS surface skin and air temperature differences ($T_s - T_a$) over West Africa. Nighttime differences are mainly governed by the longwave radiation balance, with air temperature usually

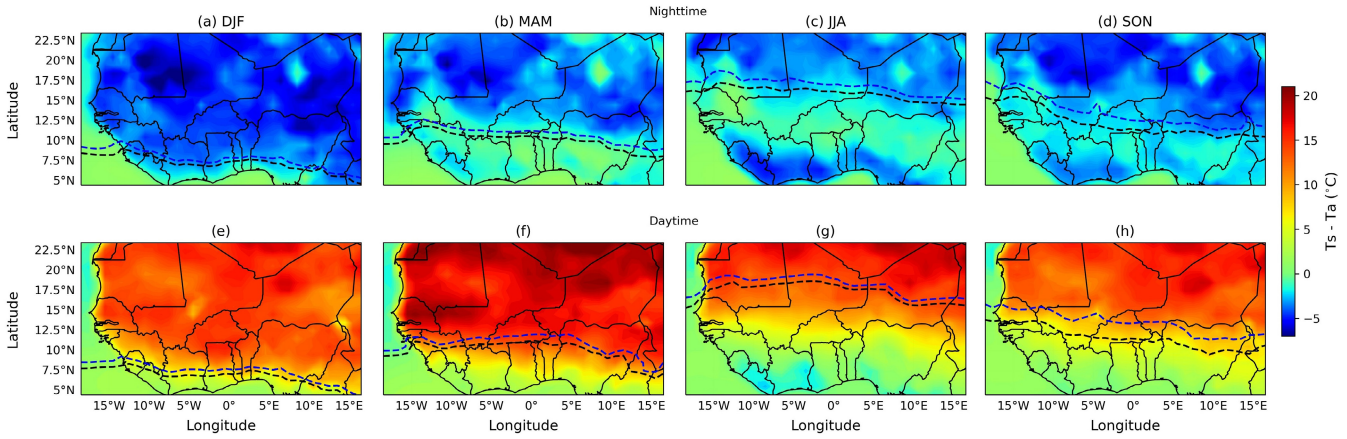

FIGURE 6 Seasonal mean of AIRS (a–d) nighttime (0130 LT) and (e–h) daytime (1330 LT) skin and air temperature differences for the period, from 2003–2018. Super-imposed are the seasonal ITD contours from q925 (10 g·kg^{-1}; blue) and Td925 (14°C; black)

higher than the skin temperature (Prigent *et al.*, 2003). This is observed in the night (Figures 6a-d), and occurs north of the ITD seasonally. The nocturnal T_a north of the ITD, is higher (Figures 6a-d), especially in DJF (Figure 6a), with secondary locations below the ITD (along the coast) in JJA (Figure 6c) and SON (Figure 6d). In JJA (Figure 6c), the maximum T_a located along the coast, may be influenced by the "little dry spell" conditions from the quasi-stationary high pressure system established in August (Parker and Diop-Kane, 2017). Furthermore, the areas below the nighttime ITD, where the skin temperature is about 2–8°C higher than the air temperature may also denote regions of the seasonal nighttime propagation of storms. That is, the nighttime high skin temperature dynamics provide sufficient nighttime conditions and instability to aid the evolution of these storms. In fact, the maximum rainfall during the monsoon period is about 200 km south of the ITD (Parker and Diop-Kane, 2017), in-line with the regions where the storms likely propagate.

Daytime surface warming increases the surface skin temperature (Figures 6e,f), which is favourable for heat and moisture fluxes. With little to no moisture available at the Savanna and Sahelian regions (see Figures 5a,b, e,f), skin temperature is elevated especially during DJF (Figure 6e) and MAM (Figure 6f) daytime, as most of the absorbed solar radiation is used for surface heating (sensible heat), instead of evapotranspiration (latent heating). In DJF, the result is cloudless and warm daytime conditions over these regions and cooler nighttime temperatures (T_a). In JJA (Figure 6g) as compared to MAM (Figure 6f), daytime T_s from the Savanna to Sahelian region reaches its minimum with the difference declining close to 7°C. This may possibly be linked to the shift in intense convection into the Sahel at this period as the ITD reaches its peak northward migration (Figure 3g). Furthermore, the warmer skin temperature may possibly have implications on storm initiation and propagation during the onset and peak monsoon seasons (MAM and JJA). For instance, Klein and Taylor (2020) found a preference for storms to initiate, intensify and propagate over drier soils (warmer T_s) as compared to the wetter soils. Based on the previous study, Taylor *et al.* (2022) have developed and shown the potential of using land surface temperature (surface skin temperature) anomalies as soil moisture proxy for nowcasting storms over West Africa.

4.4 | AIRS equivalent potential- and saturation equivalent potential temperature

The AIRS seasonal θ_e at 925–400 hPa is shown in Figure 7. For all seasons, θ_e is high, but decreases with latitude. The decline is more prominent in DJF (Figures 7a,e) and usually north of 15° N. The restriction of instability along the coast in DJF (Figures 7a,e) is positively correlated with the diurnal variability of the surface skin and air temperatures in DJF (see Figures 6a,e). That is, the warmer T_s, increases the sensible heat flux needed for evapotranspiration and convective thermals (Figures 6a,e), resulting in an unstable lower troposphere in Figures 7a,e. Minimal rainfall is observed over West Africa whenever θ_e is less than 320 K (Oduro-Afriyie, 1989). This is noticeable in the strong diurnal cycle over the Sahelian region, where θ_e falls below 320 K from the near surface to about 600 hPa in DJF (see Figures 7a,e) and daytime MAM (Figures 7f). The constant inland advection of moisture and convection from MAM to SON results in a deeper vertically unstable

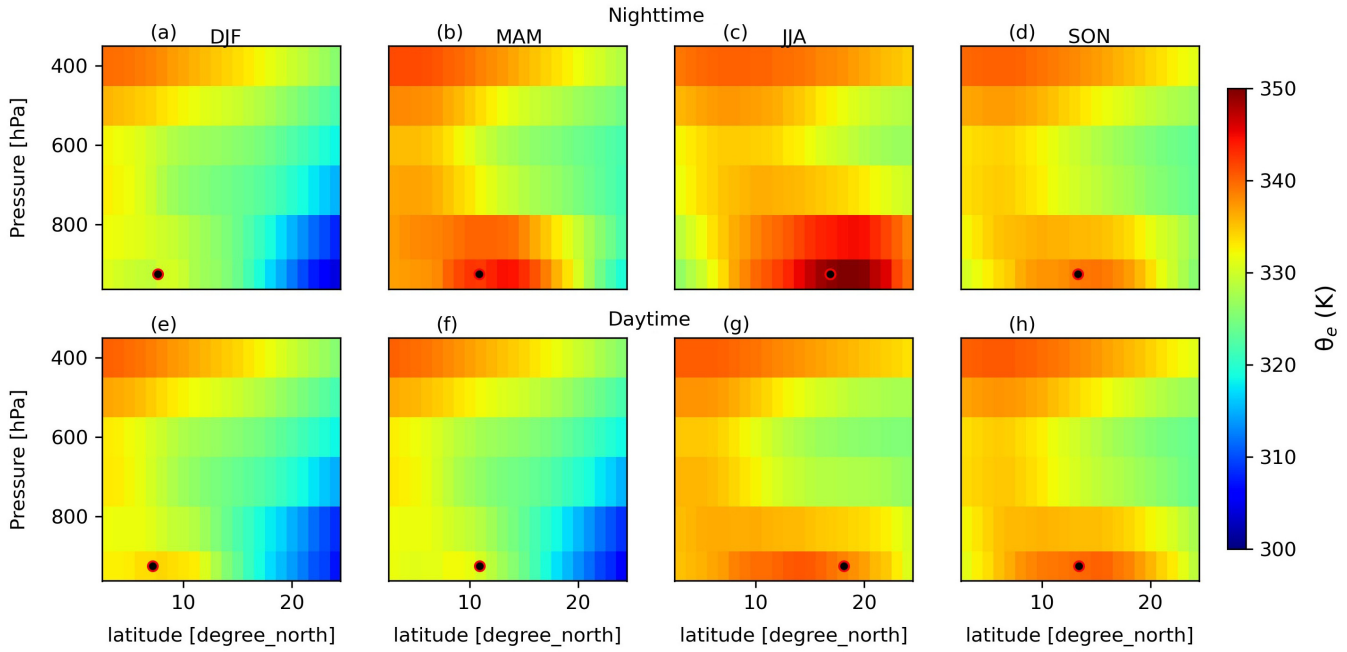

FIGURE 7 Seasonal mean of the θ_e for West Africa at AIRS nominal overpass for nighttime (0130 LT, a–d) and daytime (1330 LT, e–h) for the period, from 2003 to 2018. As in Figure 5, the seasonal zonal mean is calculated across longitudes 18.5° W–18.5° E. The circular dot shows the mean location of the ITD for the season based on 10 g·kg^{-1} from q925

troposphere from the Guinea Coast to the Sahel. For MAM, θ_e is higher over the entire Guinea Coast (5°–10° N) at night to most parts of the Sahel (Figure 7b), with a southward decline in the day (Figure 7f).

According to Thorncroft *et al.* (2003), θ_e reaches a maximum during the rainy season, around 10°–15° N. Figure 5c, agrees with the location of the maximum θ_e, and this occurs at the 925 hPa level during the night (Figure 5c) as opposed to the day (Figure 5g). The peak of nocturnal water vapour in JJA at the Sahel (Figure 5c) and instability (Figure 7c), is favoured by moderately high daytime skin temperature (Figure 6g), which allows more water vapour to be contained in the atmospheric column (Jin and Dickinson, 2010). In SON, the gradual recession of the ITD southward from the Sahel, (Figures 3d,h,l), also reduces both the high moisture content (Figures 5d,h) and instability (θ_e, Figures 7d,h). Moreover, the altitudinal variations show the mid-troposphere (700–500 hPa) has moderate θ_e, which increases marginally throughout the seasons, with peak in JJA. Elevated nocturnal θ_e is created by the meridional surge in moisture (see Figure 5), by the NLLJ, which destabilizes the lower troposphere and enhances stratus and stratocumulus cloud formations (Schrage and Fink, 2012; Schuster *et al.*, 2013; Aryee *et al.*, 2021). The impact of the destabilization or instability from the θ_e, accounts for the increasingly prominent lower tropospheric disparities in JJA diurnal cycle over the Sahel (Figures 7c,g). The magnitude of nocturnal instability also corresponds to the higher occurrence and propagation of MCSs during the night than day, with the genesis of these storms initiating during the day (Parker and Diop-Kane, 2017; Vizy and Cook, 2018; Aryee *et al.*, 2019).

Anomalies in nighttime equivalent potential temperatures are negative for all seasons in the lower to middle troposphere (Figures 8a-d). The lowest nighttime anomalies lie at or about 1° north of the seasonal nocturnal ITD. According to Omotosho (1988), negative θ_e' can correspond with dust transport. For the season of DJF (Figures 8a,e), when the Saharan dust prevails over the sub-region, this phenomena can be observed, with dryness characterizing the near surface (925 hPa) to almost 400 hPa diurnally across most latitudes. However, this may not always be the case during the summer monsoon season. For instance, negative nighttime anomalies from MAM to SON (Figures 8b–e), with minima centred north of the ITD is indicative of the seasonal belt for thunderstorm propagation. Furthermore, the negative (positive) anomalies in JJA daytime (Figure 8g) centred at the Guinea Coast (Sahel) are linked to the presiding atmospheric stability as the rain belt gradually progresses towards the Sahel. Hence, this results in a deep convective state over the Savanna to the Sahelian regions and relative dryness over the Guinea Coast. Moreover, the establishment of the "little dry spell" in JJA, from a

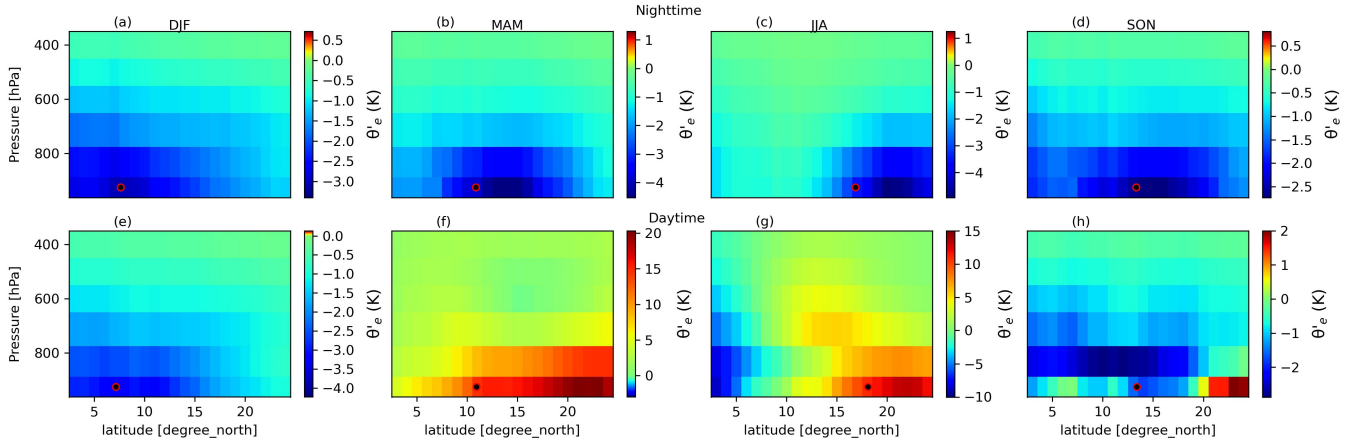

FIGURE 8 Seasonal AIRS $\theta_e^{'}$ over West Africa at nighttime (0130 LT, a–d) and daytime (1330 LT, e–h) nominal overpass times for the period, from 2003 to 2018. As in Figures 5,7, the seasonal zonal mean is calculated across longitudes 18.5° W–18.5° E. The circular dot shows the mean location of the ITD for the season based on 10 g·kg^{-1} from q925

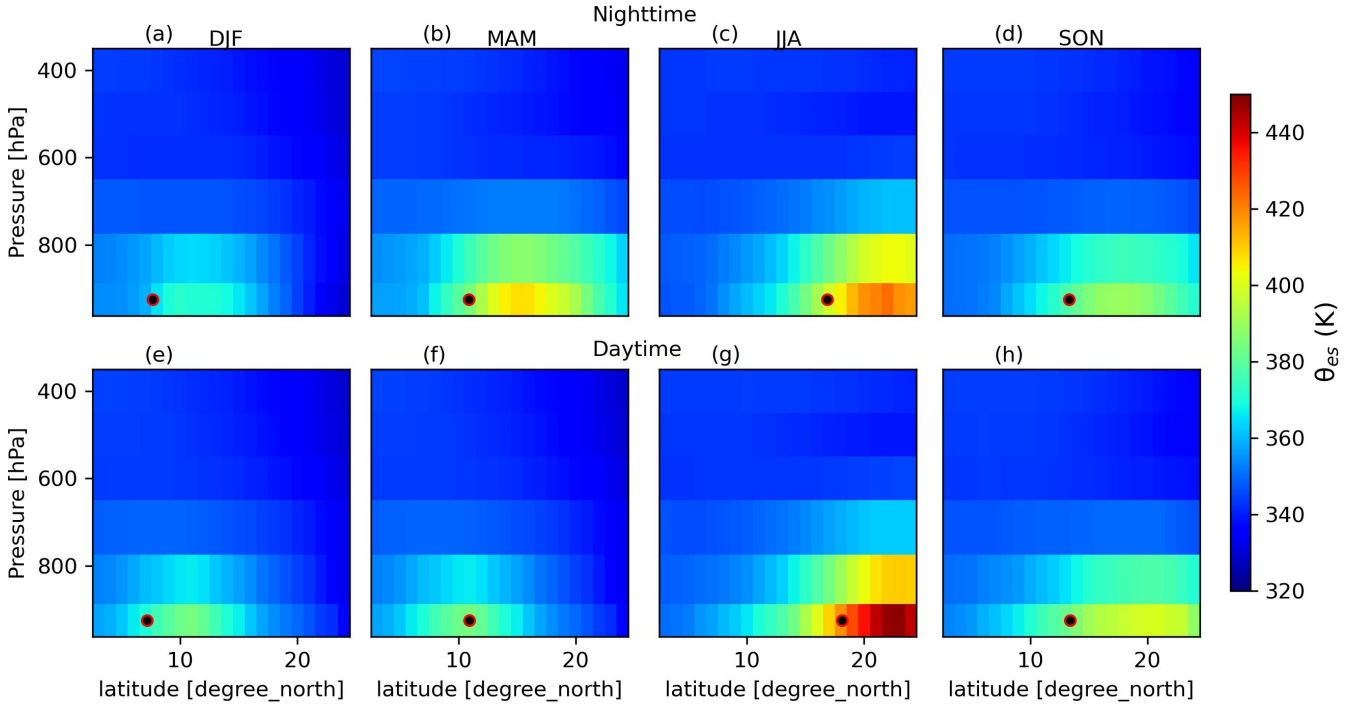

FIGURE 9 Seasonal mean of AIRS θ_{es} at nighttime (0130 LT, a–d) and daytime (1330 LT, e–h) nominal over pass times, and averaged longitudinally across 18.5° W–18.5° E. The circular dot shows the mean location of the ITD for the season based on 10 g·kg^{-1} from q925

combined effect of anticyclogenesis of the St. Helena high pressure and the northward acceleration of the ITD (Parker and Diop-Kane, 2017), may also have induced negative daytime anomalies at the Guinea Coast (≤−5 K, Figure 8g). The distribution of $\theta_e^{'}$ corroborates the findings of Omotosho (1984) and Oduro-Afriyie (1989), where the Guinea Coast had mean values ranging from −4 to −5 K and −10–15 K for the Savanna to Sahel during the monsoon period. The highly positive $\theta_e^{'}$ beyond 20° N is also indicative of the dry troposphere as observed in Figure 7f. As the rain-belt progresses southward to the Guinea Coast in the post-monsoon period (SON), both night and daytime anomalies at the lower troposphere become negative over most regions, but the corresponding θ_e (Figures 7f–h, 335–345 K) shows an unstable troposphere. This implies that, in both MAM and SON daytime cases when the rain band is located at the Guinea Coast, anomalies in MAM (positive) and SON

(negative) are of opposing signs, but significant to result in thunderstorm formations (Figure 8f,h).

For all seasons (Figure 9) except MAM daytime (Figure 9f), maximum θ_{es} lie north of the ITD position, possibly depicting relatively dry troposphere. Values of θ_{es} are as high as 450 K during the day in JJA (Figure 9g). In DJF, the nocturnal and diurnal values range between 360–380 K (Figure 9a,e). The pattern of maximum θ_{es} is usually positioned at the Savanna to Sahelian regions of West Africa. Generally, daytime anomalies are low (Figure 10), but with higher deviations in MAM daytime (Figure 10f). The deviations are located over the Sahelian region, possibly also alluding to a dry lower troposphere (Figure 5f) and intense surface skin temperature (Figure 6f) which raised the anomalies to around 60 K. In SON θ_{es}' can reach 4 K and 5 K during the night (Figure 10d) and day (Figure 10h) respectively.

4.5 | AIRS-derived thunderstorm initiation indices

The seasonality of AIRS-derived thunderstorm indices, indicating the progression of seasonal thunderstorm activities is shown in Figure 11. The indices are computed from 1330 LT data in view of the fact that convection usually begins within this period. Due to limitations in obtaining station thunderstorm observations for the entire West Africa, thresholds for thunderstorm initiation peculiar to the region could not be computed. Hence, the seasonal daytime climatology of these indices are interpreted using the general thresholds stated under Section 3.1.1. In addition, these indices are assessed on their capabilities to detect the seasonal hotspots and progression of thundery activities based on their predictability thresholds.

In DJF (Figures 11a,e,i,m), the indices show a lower chance of thunderstorm over the entire West African region, which is best captured by HI, with values exceeding 40°C (Figure 11i). This may partially be due to the sensitivity of the HI to sharp humidity gradients. On the other hand, in DJF, areas south of the ITD usually experiences isolated rainfall events, which are captured by the K-index (Figure 11a), TT-index (Figure 11 e) and DCI (Figure 11m). During monsoon onset (MAM), the deep convective region, is well captured by the DCI (Figure 11n) and TT index (Figure 11f). Averagely, the seasonal K-index also shows a 40–80% (25–35°C, Figure 11b) probability of thunderstorm occurrence located below 12° N. At the same latitude, the HI performs poorly in MAM with the recommended threshold for thunderstorm occurrence (<30°C) exceeded by 10–20°C (Figure 11j), thus implying a stable atmosphere. All indices however, show the Sahel to be moderately unstable in MAM, probaby due to occasional storm events which may track the region.

During JJA, the K-index predicts a 40–90% chance of rains from 4° N to 15° N (Figure 11c). It should be noted that, although August marks the dry spell over the Guinea Coast (Parker and Diop-Kane, 2017), the high rainfall prediction by the K-index in JJA (Figure 11c) may arise from instability in June and July only. The HI also indicated a high chance of thunderstorms especially over the Nigeria-Cameroonian border (Adamawa plateau) in JJA, as the values fell below 30°C (Figure 11k). However, HI is unable to detect the deep convective thunderstorm activities over the Sahel. The TT index (Figure 11g) and DCI (Figure 11o) on the other hand,

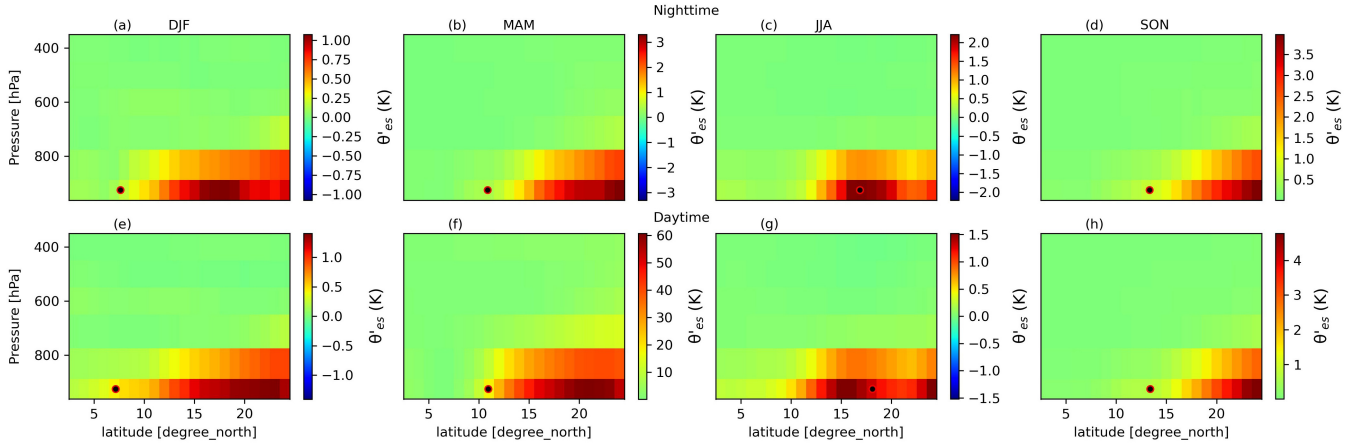

FIGURE 10 Seasonal mean θ_{es}' for West Africa at AIRS nominal overpass for nighttime (0130 LT, a–d) and daytime (1330 LT, e–h) for the period, from 2003 to 2018. As in Figures 5, 7 and 9, zonal averages are computed longitudinally across 18.5° W to 18.5° E. The circular dot shows the mean location of the ITD for the season based on 10 g·kg^{-1} from q925

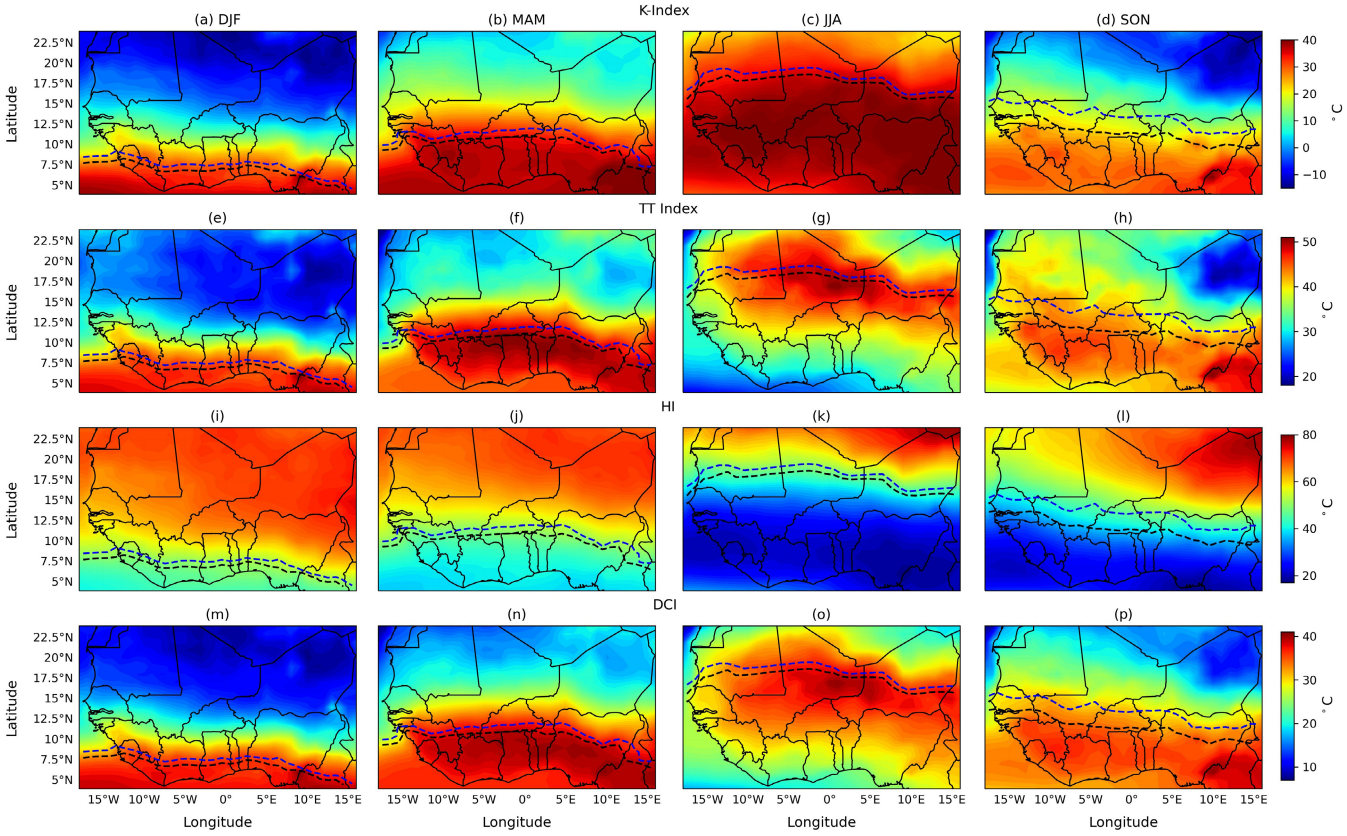

FIGURE 11 Seasonal mean AIRS-derived daytime (1330 LT) instability indices from 2003–2018 for (a–d) George's K-index (K-index), (e–h) Total totals index (TT), (i–l) humidity index (HI) and (m–p) deep convective index (DCI). Super-imposed are the seasonal ITD contours from q925 (10 g·kg^{-1}; blue) and Td925 (14°C; black)

position the deep convection only around the ITD. This is misleading as the deep convection in this season is located south of the ITD, as captured by the K-index (Figure 11c).

During SON (Figures 11d,h,l,p), all indices show the drying troposphere (progressively stable with low thunderstorm chances) over the Sahel and the unstable Guinea Coast (high thunderstorm chances). K-index (Figure 11d), TT index (Figure 11h) and DCI (Figure 11p) show maximum deep convection located at the Adamawa plateau, which corresponds with the high rainfall amounts observed in Figure S1d. Meanwhile, HI is unable to show the exact areas of deep convection in SON, but instead, indicates a higher chance of thunderstorms over the entire Gulf of Guinea region (Figure 11). The shortcomings of HI in locating thunderstorm potential in MAM and the seasonal hotspots of thunderstorm initiation, spells the need for bias-correcting AIRS HI, as undertaken previously by Ferguson and Wood (2011). Over Nigeria, higher K-index and TT-index were observed using European Center for Medium-Range Weather Forecasts Reanalysis Fifth generation datasets (Matthew *et al.*, 2021), however, the spatial structure at all seasons is similar to Figures 11a-h.

4.6 | Station thunderstorm days over Ghana and corresponding AIRS composites

Of the seven weather stations considered, Accra, Saltpond, Ho, Kumasi and Wenchi, located in the southern part of Ghana usually experience a bi-modal seasonal rainfall distribution, with peaks in March–July and September–November (see Figure S1). By contrast, stations Bole and Tamale, located to the north have a single rainfall peak, usually in September (Figure S1). In August, is the lull in rainfall which is prominently observed at the coastal and inland stations (Figure S1). Generally, the coastal stations, Accra and Saltpond, are at prime locations for all-year rainfall activities, relative to other stations considered, due to the Atlantic Ocean, coupled with sea and land breeze effects. But the prime location for rainfall does not necessarily imply higher rainfall amounts at the stations. Rainfall occurrence at the inland stations, Ho and Kumasi, is affected by orography, including river valley circulations like that of the Volta River. The topography at Wenchi, Tamale and Bole is relatively flat, with the exception of the White Volta and other minor river valleys.

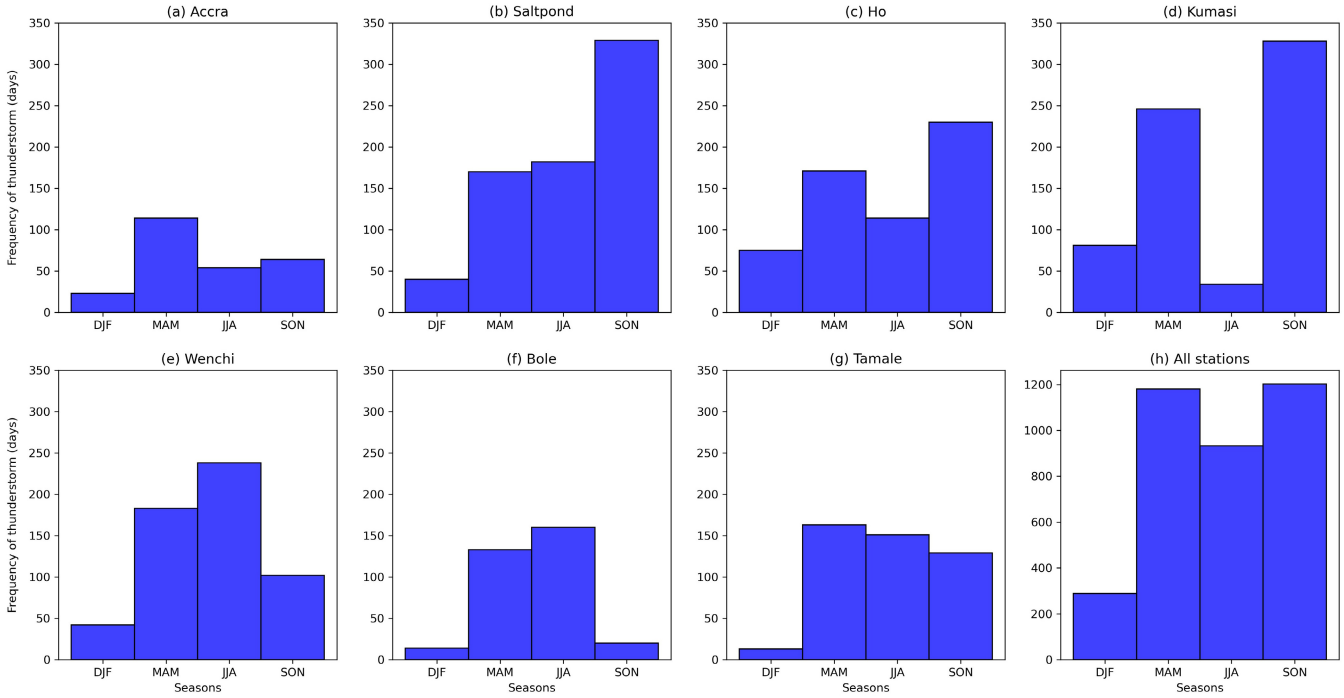

FIGURE 12 Histograms of the seasonal frequency of observed thunderstorm days reported by Ghana meteorological agency forecasting observers stationed at (a) Accra, (b) Saltpond, (c) Ho, (d) Kumasi, (e) Wenchi, (f) Bole and (g) Tamale for 2003–2009 and 2015–2018. At panel (h) is the seasonal count of thunderstorm samples at all stations. It should be noted that only thunderstorms associated with rainfall are included, thus dry thunderstorm days do not form part of the analysis. For clarity, the y-axis limit at each station (a–g) has been scaled to the maximum thunderstorm frequency

4.6.1 | Seasonality of thunderstorms at select stations

Figures 12a–g shows the seasonal frequency of thunderstorm days at the selected stations over Ghana. The frequency distribution (in days) is the count of reported thunderstorm days between 2003–2009 and 2015–2018 at the synoptic stations. For clarity, a day is defined to be a thunderstorm day if any of the seven Ghana stations report a thunderstorm associated with rainfall (i.e., wet thunderstorm) on that day. Ho (Figure 12c) and Kumasi (Figure 12d) have the greatest frequency of DJF thunderstorm events (≈75 days), whereas Tamale has the least (Figure 12g; ≈13 days). At Saltpond (Figure 12b), Ho (Figure 12c) and Kumasi (Figure 12d), the thunderstorm peak occurs in the post-monsoon season (SON). The lull in thunderstorm activities at some southern stations in JJA (Figures 12a,c–d) is attributable to the impact of the retreat of the ITD northward in August. This implies that, the majority of JJA thunderstorm events at these southern stations (Figures 12a,c–d) occur in June and July and not August, as also observed in Figure S1.

Interestingly, across all seasons, thunderstorm events are more frequent at Saltpond (Figure 12b) than Accra (Figure 12a), although both stations lie along the coast (central and east respectively). The corresponding rainfall amounts are also higher at Saltpond than Accra (Figure S1). According to forecasters from the Ghana Meteorological Agency, the low frequency of thunderstorms over Accra as compared to other coastal stations result from the orientation of the coastline. Such that, the coastal orientation leads to winds blowing parallel to the eastern coast (Accra) which diverts most storms away from the area, and perpendicular to the central (Saltpond) and western coasts, which favours storm tracks. In fact, Bryson and Kuhn (1961) found that, a gradient level flow parallel to the coast will be associated with divergence within the friction layer, resulting in significant rainfall reductions. Others such as: Brongersma-Sanders (1971), Malda *et al.* (2007), Chen *et al.* (2014), Kim *et al.* (2020), and Zeng and Wang (2022) also concluded that the coastline structure has profound impact on MCS propagation and wind direction via land-ocean differential friction, wind shear, surface convergence/divergence and upwelling effects.

The impact of the lull in August which determines the rainfall seasonality (uni[bi]-modal; Figure S1) does not strictly affect the corresponding thunderstorm

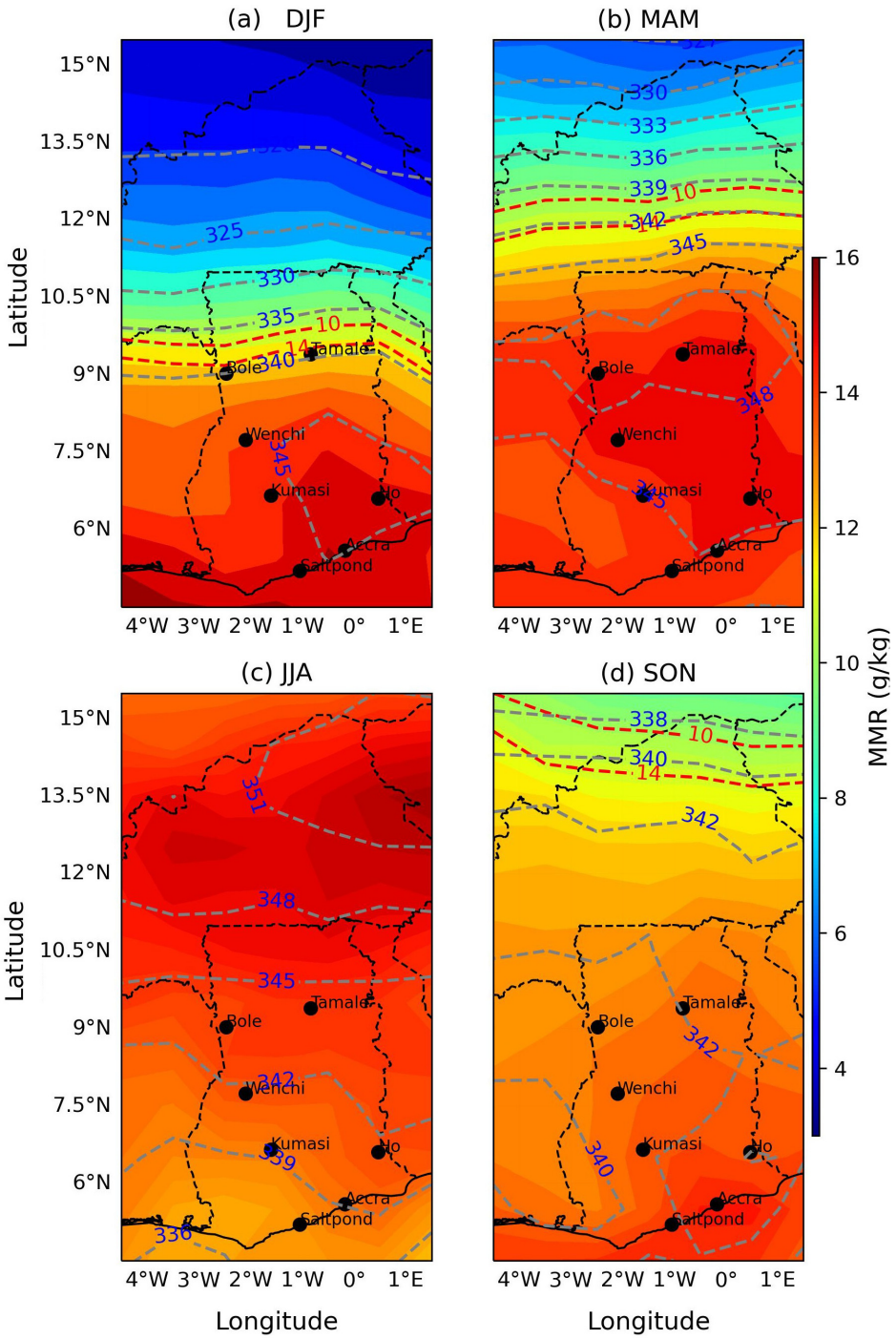

FIGURE 13 Composite seasonal mean of the AIRS low-level moisture (925 hPa) to mid-level (600 hPa), tropospheric MMR, θ_e contours (grey dashed) and 10 g·kg^{-1} and 14°C ITDs (dashed red) on wet thunderstorm days at the selected stations over Ghana between 2003–2009 and 2015–2018. Analysis is performed on the daytime overpass only, and the total number of wet thunderstorm samples used for the composites is shown in Figure 12h

seasonality. For instance, at the southern stations, whereas the thunderstorm frequency at Accra (Figure 12a), Ho (Figure 12c) and Kumasi (Figure 12d) are clearly bi-modal, Saltpond (Figure 12b) and Wenchi (Figure 12e) are uni-modal, along with Bole (Figure 12f) and Tamale (Figure 12g). It is known that the cessation of the rainfall over the Northern stations is usually between the third dekad of September to the first dekad of October (Amekudzi *et al.*, 2015) and possibly November (Dunning *et al.*, 2016). Scatterplots of the average thunderstorm initiation indices versus the thunderstorm frequency, at all stations and seasons is shown in Figure S2. From Figure S2, the mean lower and upper limits of the K-index, TT-index, HI, and DCI values ranged from 25 to 34°C, 38 to 47°C, 18 to 33°C, and 30 to 39°C, respectively, on thunderstorm days over Ghana. Note that for the TT-index, for example, this range differs from the range of 44–50°C suggested by Miller (1975).

4.6.2 | AIRS MMR and equivalent potential temperature composites

Figure 13 shows the composite cross-sectional mean of the seasonal equivalent potential temperature, mass mixing ratio from 925 hPa to 600 hPa and the mean location of the ITD during thunderstorm days over the selected stations in Ghana. For all seasons except JJA, the mean latitude of the ITD on thunderstorm days is shown to be north of its climatological position (compare Figures 3e–h with Figure 13). In DJF, the ITD during thunderstorm days is positioned around 10° N (Figure 13a), whereas the climatological mean position over Ghana is around 7° N (Figure 3e). This results in an approximate 3° northward surge anomaly on the thunderstorm days. The anomalous northward displacement of the ITD in DJF has been attributed to the interaction of the feature with the mid-latitude trough (Parker and Diop-Kane, 2017), and upper-level trough (Knippertz and Fink, 2009; Ward *et al.*, 2021). It is found over West Africa that, December–March days in the upper quintile of upper-level trough strength occur when the ITD is displaced on-average 1.5° north of its climatological position (Ward *et al.*, 2022). The cumulative effect of all interactions on thunderstorm days, is a surge in moisture south of the ITD, and hence the northward acceleration of the ITD.

For the transition seasons, ITD is displaced about 0.2° northward in MAM (Figure 13b), and about 2° northward in SON (Figure 13d). In MAM, the displacement in March may be very substantial like in DJF, but substantial in April–May, which explains the small net change for MAM. In JJA, the ITD is already positioned too far north (≈18° N, Figure 3g) to have any significant impact on the stations studied, or storms that form over the Guinea Coast (Figure 13c). In fact, the ITD anomaly was found to be around 1.2° south of the climatology in JJA, but again, this southward retreat of the ITD on the storm days may have had no impact on moisture transport to the stations. For instance, based on Table 1, the maximum displacement of the ITD on the storm days, as compared to the station latitude ranged between 9° and 10° north at Accra, Saltpond, Ho and Kumasi. In the DJF, the maximum displacement for both ITD estimates is observed at Saltpond (q925: 3° north, Td925: 2.2° north), with the least displacement observed at Tamale (q925: 0.1° south) and Bole (Td925: 1° south). Meanwhile, in MAM and SON (Table 1), the ITD is located close (minimum offset) to the Northern stations, including Wenchi, as compared to all other stations.

Figure 13a also shows increased moisture content (≈16 g·kg^{-1}) at the coastal to middle stations and moderately high content (≈14 g·kg^{-1}) at the Northern stations during thunderstorm events. This shows that for the dry period in DJF, the in-flow of moisture on thunderstorm days extends vertically to the mid-troposphere to sustain storm growth. In MAM (Figure 13b), there is a larger spatial coverage of elevated moisture, extending from the Southern to the Northern stations. Meanwhile, moisture amounts decline to about 13–14 g·kg^{-1} in JJA, favouring the Northern stations. The lower amount of moisture in JJA, as previously stated may be due to the ITD positioned further north from these stations and hence, the higher moisture depth also located within this zone. SON moisture (Figure 13d) averages are similar to JJA, however the maxima occurs at the Southern as compared to the Northern stations. The θ_e at the stations, in all seasons were higher than the climatological values in Figures 7e–h.

The overall composite anomalies of the vertical profile of AIRS seasonal MMR and θ_e on thunderstorm days at the selected synoptic stations in Ghana are shown in Figures 14a–n. During the dry season (DJF, blue dashes), MMR on thunderstorm days is anomalously high at all stations (Figures 14a–g), up to about 7–8 g·kg^{-1} at the Northern stations of Bole and Tamale (Figures 14f,g). Particularly at these stations, the anomalously high moisture in DJF destabilizes the lower troposphere (Figures 14m,n). Meanwhile in MAM - SON, the lower tropospheric MMR anomalies are relatively low (Figures 14a–g), but usually associated with strong low-level destabilization (Figures 14h–n). Positive mid-tropospheric (700–500 hPa) moisture anomalies on thunderstorm days also contribute to instability, as well as increased buoyancy, except at Bole and Tamale (Figures 14m,n). The lower troposphere becomes highly unstable, with θ_e' peaking between 10–25 K at the northernmost stations. These heating peaks can be associated with maximum vertical transport during the day, an indication of a deep convective boundary layer that maintains baroclinicity (Parker *et al.*, 2005). The vertical profile of θ_e' also show a distinct vertical orientation at the stations. Thus, except for DJF, the anomalies increase from the 925 to 600 hPa from Accra to Wenchi (Figures 14h–l), but shows an overall decreasing profile at Bole and Tamale (Figures 14m,n). Since the θ_e equation (see Equation 7) consists of air temperature and humidity (moisture; MMR), we compared the vertical patterns of their anomalies (Figures 14a–g, o–u) in a strictly qualitative exercise to determine which of the two variable anomaly profiles lie in-phase with that of θ_e' (Figures 14h–n). In DJF, the humidity profile (Figures 14a–g) is the dominate signal at all stations due to the sudden moisture upsurge. Then, from MAM - SON, the humidity is important over the coastal (Accra and Saltpond; Figures 14a,b) and Northern stations

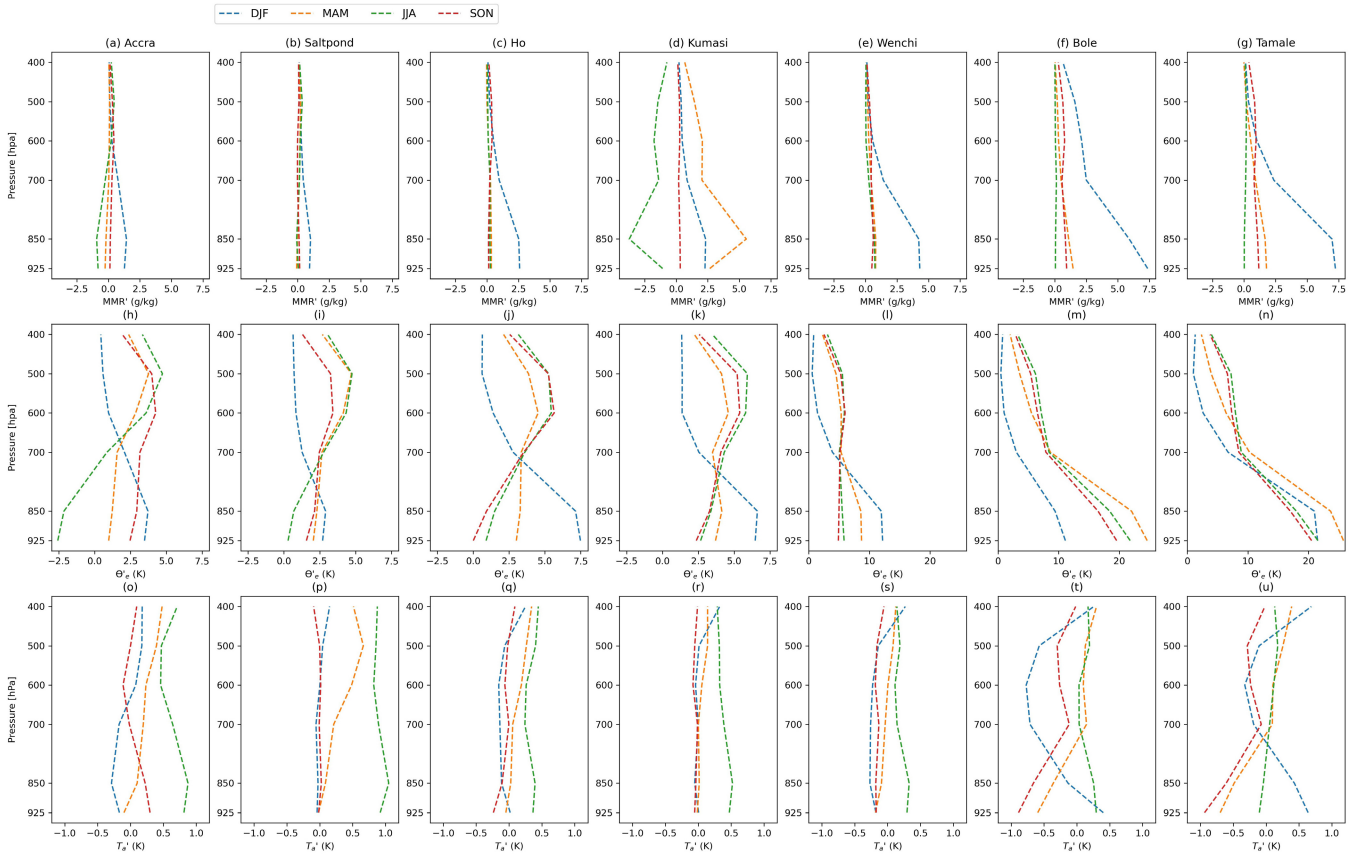

FIGURE 14 Seasonal composite of AIRS-derived 1330 LT $MMR^{'}$ (a–g), $\theta_e^{'}$ (h–n) and $T_a^{'}$ (o–u) vertical profiles on observed wet thunderstorm days during 2003–2009 and 2015–2018 at the seven Ghana weather stations. Here, the AIRS anomaly and climatology composites (2003–2009 and 2015–2018) are calculated using data from the $1^{\circ} \times 1^{\circ}$ AIRS3STD grid within which the respective station lies. The thunderstorm day sample sizes are illustrated in Figure 12a–g

TABLE 2 A summary of whether on thunderstorm days for a given station and season, the temperature ($T_a^{'}$) and/or humidity ($MMR^{'}$) profile(s) match that of the $\theta_e^{'}$ (Figure 14)

Seasons	Accra	Saltpond	Ho	Kumasi	Wenchi	Bole	Tamale
DJF	Humidity	Humidity	Humidity	Humidity	Humidity	Humidity	Humidity
MAM	Both	Both	Temperature	Temperature	Humidity	Humidity	Humidity
JJA	Humidity	Humidity	Temperature	Temperature	None	Temperature	None
SON	Humidity	Temperature	Temperature	Temperature	Humidity	Humidity	Humidity

Note: When only one variable matches in profile, it may be of greater relative importance in terms of forecasting thunderstorms.

(Bole and Tamale; Figures 14f,g), whereas temperature anomalies ($T_a^{'}$) tend to dominate the $\theta_e^{'}$ response at inland stations (Ho and Kumasi; Figures 14q,r). Table 2 gives a summary of whether $T_a^{'}$ and/or $MMR^{'}$ variable(s), based on Figures 14a–g,o–u, has a vertical pattern similar to the $\theta_e^{'}$ profiles (Figures 14h–n).

5 | CONCLUSIONS

Understanding the thermodynamics and evolution of the West African monsoon is essential for improving weather forecasting techniques in the region. In this study, we analysed the observation of West Africa's moist convective environment from AIRS thermodynamic fields at seasonal timescales from 2003 to 2018, relative to the progression of the ITD. The moist convective variables considered were the surface skin and air temperatures, equivalent potential temperature, saturation equivalent potential temperature, and the mass mixing ratio.

The results show that AIRS data products capture the seasonality of West Africa's moist convective environment, consistent with prior observationally-based studies

and our knowledge of the local weather. Seasonally, the AIRS derived ITD methods show a higher northward latitudinal position of the 10 $g{\cdot}kg^{-1}$ (q925) contour as compared to the 14°C (Td925) contour. The onset of the monsoon at the Guinea Coast in MAM is associated with extremely high skin temperature north of the ITD as compared to other seasons. The establishment of the quasi-stationary high pressure system at the peak of the monsoon (JJA), raises daytime surface air temperature due to prevailing low clouds which may warm the lower troposphere along the Guinea Coast. AIRS-derived equivalent potential temperature shows an unstable lower troposphere, which progresses northward during the nighttime. Anomalies in θ_e are higher during the day than at night and can aid in detecting and monitoring convection and storms over the region. The K-index (Figures 11a–d) is the most skillful thunderstorm index in the study domain, and hence, should be considered for seasonal forecasting of deep convective precipitation. For AIRS-derived regional thunderstorm thresholds of the indices over Ghana, ranges were found as: 25–34°C (K-index), 38–47°C (TT-index), 18–33°C (HI) and 30–39°C (DCI). However, further studies are needed on the predictability of the indices, especially, the K-index on the daily timescale to aid daily weather forecasting over West Africa. AIRS MMR' and θ_e' at the seven synoptic stations in Ghana are strongly positive, and show distinct vertical orientation from the 925–400 hPa on thunderstorm days. The ITD on thunderstorm days is also anomalously displaced northward in DJF, MAM and SON, as compared to the climatological positions, but southward in JJA.

Based on the results from the study, AIRS provides a valuable climatological record of the seasonal movement of the ITD and its influence on large-scale atmospheric temperature, humidity, and thunderstorm potential. The possibility of assimilating AIRS products or the European Space Agency Infrared Atmospheric Sounding Interferometer (Hilton *et al.*, 2009) into the WRF or COSMO models could complement weather forecasting procedures in West Africa, including daily nowcasts. Moreover, future studies could explore using the past AIRS-IFS variable relationships to bias-correct future IFS seasonal rainfall forecasts.

AUTHOR CONTRIBUTIONS

Marian Amoakowaah Osei: Conceptualization; data curation; formal analysis; investigation; methodology; visualization; writing – original draft; writing – review and editing. **Craig Ferguson:** Conceptualization; supervision; writing – review and editing. **Emmanuel Quansah:** Writing – review and editing. **Michael Padi:** Resources. **Leonard Kofitse Amekudzi:** Funding acquisition; supervision; writing – review and editing. **Sylvester K. Danuor:** Funding acquisition; project administration.

ACKNOWLEDGEMENTS

The authors would like to acknowledge the GCRF African SWIFT project for funding this research. This work was supported by UK Research and Innovation as part of the Global Challenges Research Fund, grant number NE/P021077/1. We also thank the Ghana Meteorological Agency for making their thunderstorm data available for this study, and Prof. Douglas Parker of the University of Leeds on his insight on the ITD. We would also like to thank the Royal Society for supporting the first author with the Newton International Fellowship, with grant reference number NIF\R1\211183 during the final stages of this manuscript. We are also grateful to our anonymous reviewer for the useful comments and criticisms which helped shape the manuscript into its final form.

CONFLICT OF INTEREST

Authors declare no conflict of interests.

ORCID

Marian Amoakowaah Osei https://orcid.org/0000-0003-3481-7222
Craig R. Ferguson https://orcid.org/0000-0003-0821-5922
Emmanuel Quansah https://orcid.org/0000-0002-3382-1775
Michael Padi https://orcid.org/0000-0001-8523-4110
Leonard K. Amekudzi https://orcid.org/0000-0002-2186-3425
Sylvester Danuor https://orcid.org/0000-0001-6908-1935

REFERENCES

Akinsanola, A. and Ogunjobi, K. (2013) Equivalent potential temperature: a diagnostic tool for cold spells signature in Nigeria. In: *International Conference Proceedings of the Nigerian Meteorological Society*. Abuja Nigeria.

Amekudzi, L.K., Yamba, E.I., Preko, K., Asare, E.O., Aryee, J., Baidu, M. and Codjoe, S.N. (2015) Variabilities in rainfall onset, cessation and length of rainy season for the various agro-ecological zones of Ghana. *Climate*, 3, 416–434.

Aryee, J., Amekudzi, L., Atiah, W., Osei, M. and Agyapong, E. (2019) Overview of surface to near-surface atmospheric profiles over selected domain during the QWeCI project. *Meteorology and Atmospheric Physics*, 131, 1067–1081.

Aryee, J.N., Amekudzi, L.K. and Yamba, E.I. (2021) Low-level cloud development and diurnal cycle in southern West Africa during the DACCIWA field campaign: case study of Kumasi supersite, Ghana. *Journal of Geophysical Research: Atmospheres*, 126, e2020JD034028.

Bolton, D. (1980) The computation of equivalent potential temperature. *Monthly Weather Review*, 108, 1046–1053.

Bou Karam, D., Flamant, C., Knippertz, P., Reitebuch, O., Pelon, J., Chong, M. and Dabas, A. (2008) Dust emissions over the Sahel associated with the West African monsoon intertropical discontinuity region: a representative case-study. *Quarterly Journal of the Royal Meteorological Society: A journal of the atmospheric*

sciences, applied meteorology and physical oceanography, 134, 621–634.

Bou Karam, D., Flamant, C., Tulet, P., Chaboureau, J.-P., Dabas, A. and Todd, M.C. (2009a) Estimate of Sahelian dust emissions in the intertropical discontinuity region of the West African monsoon. *Journal of Geophysical Research: Atmospheres*, 114, 1–14.

Bou Karam, D., Flamant, C., Tulet, P., Todd, M.C., Pelon, J. and Williams, E. (2009b) Dry cyclogenesis and dust mobilization in the intertropical discontinuity of the West African monsoon: a case study. *Journal of Geophysical Research: Atmospheres*, 114, 1–14.

Brongersma-Sanders, M. (1971) Origin of major cyclicity of evaporites and bituminous rocks: an actualistic model. *Marine Geology*, 11, 123–144.

Bryson, R.A. and Kuhn, P.M. (1961) Stress-Differential Induced Divergence with Application to Littoral Precipitation (Durch Beanspruchungsdifferenzial hervorgerufene Divergenz in ihrer Anwendung auf Niederschläge an Küsten). *Erdkunde*, 15, 287–294.

Chen, X., Zhao, K. and Xue, M. (2014) Spatial and temporal characteristics of warm season convection over Pearl River Delta region, China, based on 3 years of operational radar data. *Journal of Geophysical Research: Atmospheres*, 119, 12–447.

Dunning, C.M., Black, E.C. and Allan, R.P. (2016) The onset and cessation of seasonal rainfall over Africa. *Journal of Geophysical Research: Atmospheres*, 121, 11–405.

Ferguson, C.R. and Wood, E.F. (2010) An evaluation of satellite remote sensing data products for land surface hydrology: Atmospheric InfraRed Sounder. *Journal of Hydrometeorology*, 11, 1234–1262.

Ferguson, C.R. and Wood, E.F. (2011) Observed land–atmosphere coupling from satellite remote sensing and reanalysis. *Journal of Hydrometeorology*, 12, 1221–1254.

Flamant, C., Knippertz, P., Parker, D.J., Chaboureau, J.-P., Lavaysse, C., Agusti-Panareda, A. and Kergoat, L. (2009) The impact of a mesoscale convective system cold pool on the northward propagation of the intertropical discontinuity over West Africa. *Quarterly Journal of the Royal Meteorological Society: A journal of the atmospheric sciences, applied meteorology and physical oceanography*, 135, 139–159.

George, J.J. (1960) *Weather Forecasting for Aeronautics*. Cambridge: Academic press.

Georgiev, C., Santurette, P. and Maynard, K. (2016) *Weather Analysis and Forecasting: Applying Satellite Water Vapor Imagery and Potential Vorticity Analysis*. Cambridge: Academic Press.

Giaiotti, D.B., Steinacker, R. and Stel, F. (2007) *Atmospheric Convection: Research and Operational Forecasting Aspects*, Vol. 475. New York: Springer Science & Business Media.

Grieser, J. (2012) Convection parameters. Selbstverl.

Hastenrath, S. (2012) Contemporary climate and circulation of the tropics. In: *Climate and Circulation of the Tropics*. Chichester: John Wiley & Sons Ltd, pp. 34–43.

Hilton, F., Atkinson, N., English, S. and Eyre, J. (2009) Assimilation of IASI at the met Office and assessment of its impact through observing system experiments. *Quarterly Journal of the Royal Meteorological Society: A journal of the atmospheric sciences, applied meteorology and physical oceanography*, 135, 495–505.

Holton, J.R. (1973) An introduction to dynamic meteorology. *American Journal of Physics*, 41, 752–754.

Jacovides, C. and Yonetani, T. (1990) An evaluation of stability indices for thunderstorm prediction in greater Cyprus. *Weather and Forecasting*, 5, 559–569.

Jin, M., Dickinson, R. and Vogelmann, A. (1997) A comparison of CCM2–BATS skin temperature and surface-air temperature with satellite and surface observations. *Journal of Climate*, 10, 1505–1524.

Jin, M. and Dickinson, R.E. (2010) Land surface skin temperature climatology: benefitting from the strengths of satellite observations. *Environmental Research Letters*, 5, 044004.

Kim, S., Matyas, C.J. and Yan, G. (2020) Rainfall symmetry related to moisture, storm intensity, and vertical wind shear for tropical cyclones landfalling over the US gulf coastline. *Atmosphere*, 11, 895.

Klein, C. and Taylor, C.M. (2020) Dry soils can intensify mesoscale convective systems. *Proceedings of the National Academy of Sciences*, 117, 21132–21137.

Knippertz, P. and Fink, A.H. (2009) Prediction of dry-season precipitation in tropical West Africa and its relation to forcing from the extratropics. *Weather and Forecasting*, 24, 1064–1084.

Knippertz, P. and Todd, M.C. (2012) Mineral dust aerosols over the Sahara: meteorological controls on emission and transport and implications for modeling. *Reviews of Geophysics*, 50, 1–28.

Lothon, M., Saïd, F., Lohou, F. and Campistron, B. (2008) Observation of the diurnal cycle in the low troposphere of West Africa. *Monthly Weather Review*, 136, 3477–3500.

Malda, D., Vilà-Guerau de Arellano, J., Van Den Berg, W. and Zuurendonk, I. (2007) The role of atmospheric boundary layer-surface interactions on the development of coastal fronts. In: *Annales Geophysicae*, Vol. 25. Gottingen, Germany: Copernicus GmbH, pp. 341–360.

Matthew, O.J., Abiye, O.E. and Ayoola, M.A. (2021) Assessment of static stability indices and related thermodynamic parameters for predictions of atmospheric convective potential and precipitation over Nigeria. *Meteorology and Atmospheric Physics*, 133, 675–691.

May, P.T. and Ballinger, A. (2007) The statistical characteristics of convective cells in a monsoon regime (Darwin, northern Australia). *Monthly Weather Review*, 135, 82–92.

May, R.M., Goebbert, K.H., Thielen, J.E., Leeman, J.R., Camron, M. D., Bruick, Z., Bruning, E.C., Manser, R.P., Arms, S.C. and Marsh, P.T. (2022) MetPy: a meteorological python library for data analysis and visualization. *Bulletin of the American Meteorological Society*, 103, E2273–E2284.

Menzel, W.P., Schmit, T.J., Zhang, P. and Li, J. (2018) Satellite-based Atmospheric Infrared Sounder development and applications. *Bulletin of the American Meteorological Society*, 99, 583–603.

Miller, R.C. (1975) *Notes on Analysis and Severe-Storm Forecasting Procedures of the Air Force Global Weather Central*, Vol. 200. Air Weather Service (MAC), Scott Air Force Base, USA.

Oduro-Afriyie, K. (1989) On the mean monthly equivalent potential temperature and rainfall in West Africa. *Theoretical and Applied Climatology*, 39, 188–193.

Olsen, E., Elliott, D., Fetzer, E., Manning, E., Blaisdell, J., Susskind, J. and Iredell, L. (2017) *AIRS/AMSU/HSB version 6 data disclaimer*. NASA, Jet Propulsion Laboratory, California Institute of Technology, Pasadena, CA: Goddard Space Flight Center.

Omotosho, J. (1984) Spatial and seasonal variation of line squalls over West Africa. *Archives for meteorology, geophysics, and bioclimatology, Series A*, 33, 143–150.

Omotosho, J.B. (1988) *Energetics Study of West African Dust Haze*. International Centre for Theoretical Physics: Tech. rep.

Omotosho, J.B., Balogun, A. and Ogunjobi, K. (2000) Predicting monthly and seasonal rainfall, onset and cessation of the rainy season in West Africa using only surface data. *International Journal of Climatology: A Journal of the Royal Meteorological Society*, 20, 865–880.

Osei, M.A., Amekudzi, L.K., Ferguson, C.R. and Danuor, S.K. (2020) Inter-comparison of AIRS temperature and relative humidity profiles with AMMA and DACCIWA radiosonde observations over West Africa. *Remote Sensing*, 12, 2631.

Pante, G. and Knippertz, P. (2019) Resolving Sahelian thunderstorms improves mid-latitude weather forecasts. *Nature Communications*, 10, 1–9.

Parker, D., Burton, R., Diongue-Niang, A., Ellis, R., Felton, M., Taylor, C., Thorncroft, C., Bessemoulin, P. and Tompkins, A. (2005) The diurnal cycle of the West African monsoon circulation. *Quarterly Journal of the Royal Meteorological Society: A journal of the atmospheric sciences, applied meteorology and physical oceanography*, 131, 2839–2860.

Parker, D.J. and Diop-Kane, M. (2017) *Meteorology of Tropical West Africa: The forecasters' Handbook*. Chichester: John Wiley & Sons.

Parker, D.J., Willetts, P., Birch, C., Turner, A.G., Marsham, J.H., Taylor, C.M., Kolusu, S. and Martin, G.M. (2016) The interaction of moist convection and mid-level dry air in the advance of the onset of the Indian monsoon. *Quarterly Journal of the Royal Meteorological Society*, 142, 2256–2272.

Pospichal, B., Karam, D., Crewell, S., Flamant, C., Hünerbein, A., Bock, O. and Saïd, F. (2010) Diurnal cycle of the intertropical discontinuity over West Africa analysed by remote sensing and mesoscale modelling. *Quarterly Journal of the Royal Meteorological Society*, 136, 92–106.

Prigent, C., Aires, F. and Rossow, W.B. (2003) Land surface skin temperatures from a combined analysis of microwave and infrared satellite observations for an all-weather evaluation of the differences between air and skin temperatures. *Journal of Geophysical Research: Atmospheres*, 108, 1–14.

Roberts, A.J., Marsham, J.H. and Knippertz, P. (2015) Disagreements in low-level moisture between (re) analyses over summertime West Africa. *Monthly Weather Review*, 143, 1193–1211.

Schrage, J.M. and Fink, A.H. (2012) Nocturnal continental low-level stratus over tropical West Africa: observations and possible mechanisms controlling its onset. *Monthly Weather Review*, 140, 1794–1809.

Schuster, R., Fink, A.H. and Knippertz, P. (2013) Formation and maintenance of nocturnal low-level stratus over the southern West African monsoon region during AMMA 2006. *Journal of the Atmospheric Sciences*, 70, 2337–2355.

Sikora, C.R. (1976) *An Investigation of Equivalent Potential Temperature as a Measure of Tropical Cyclone Intensity*. Fleet Weather Central/Joint Typhoon Warning Center FPO San Francisco: Tech. rep, p. 96630.

Son, J.-H. and Seo, K.-H. (2020) Mechanisms for the climatological characteristics and interannual variations of the Guinea coast precipitation: early summer West African monsoon. *Atmosphere*, 11, 396.

Sultan, B., Janicot, S. and Drobinski, P. (2007) Characterization of the diurnal cycle of the West African monsoon around the monsoon onset. *Journal of Climate*, 20, 4014–4032.

Susskind, J. (2006) Improved soundings and error estimates using AIRS/AMSU data. In: *Algorithms and Technologies for Multispectral, Hyperspectral, and Ultraspectral Imagery XII*, Vol. 6233. Bellingham: SPIE, pp. 443–454.

Susskind, J., Blaisdell, J.M. and Iredell, L. (2014) Improved methodology for surface and atmospheric soundings, error estimates, and quality control procedures: the Atmospheric Infrared Sounder science team version-6 retrieval algorithm. *Journal of Applied Remote Sensing*, 8, 084994.

Susskind, J., Schmidt, G., Lee, J. and Iredell, L. (2019) Recent global warming as confirmed by AIRS. *Environmental Research Letters*, 14, 044030.

Taylor, C.M., Klein, C., Dione, C., Parker, D.J., Marsham, J., Diop, C.A., Fletcher, J., Chaibou, A.A.S., Nafissa, D.B., Semeena, V.S., et al. (2022) Nowcasting tracks of severe convective storms in West Africa from observations of land surface state. *Environmental Research Letters*, 17, 034016.

Thorncroft, C., Parker, D., Burton, R., Diop, M., Ayers, J., Barjat, H., Devereau, S., Diongue, A., Dumelow, R., Kindred, D., et al. (2003) The JET2000 project: aircraft observations of the African easterly JET and African easterly waves: aircraft observations of the African easterly jet and African easterly waves. *Bulletin of the American Meteorological Society*, 84, 337–352.

Vizy, E.K. and Cook, K.H. (2018) Mesoscale convective systems and nocturnal rainfall over the West African Sahel: role of the inter-tropical front. *Climate Dynamics*, 50, 587–614.

Ward, N., Fink, A.H., Keane, R.J., Guichard, F., Marsham, J.H., Parker, D.J. and Taylor, C.M. (2021) Synoptic timescale linkage between midlatitude winter troughs Sahara temperature patterns and northern Congo rainfall: a building block of regional climate variability. *International Journal of Climatology*, 41, 3153–3173.

Ward, N., Fink, A.H., Keane, R.J. and Parker, D.J. (2022) Upper-level midlatitude troughs in boreal winter have an amplified low-latitude linkage over Africa. *Atmospheric Science Letters*, e1129.

Zeng, Z. and Wang, D. (2022) Observations of heavy short-term rainfall hotspots associated with warm-sector episodes over coastal South China. *Atmospheric Research*, 106273.

SUPPORTING INFORMATION

Additional supporting information can be found online in the Supporting Information section at the end of this article.

How to cite this article: Osei, M. A., Ferguson, C. R., Quansah, E., Padi, M., Amekudzi, L. K., & Danuor, S. (2023). West Africa's moist convective environment as observed by the Atmospheric InfraRed Sounder (AIRS). *International Journal of Climatology*, *43*(5), 2428–2448. https://doi.org/10.1002/joc.7983